CHAPTER

8

Turbulence modeling

Compressible wall-bounded flows

Rene Pecnik and Asif Manzoor Hasan

Process and Energy Department, Delft University of Technology, Delft, Netherlands

8.1 Introduction

Turbulence modeling is an essential aspect of computational fluid dynamics (CFD) simulations. While direct numerical simulation (DNS) and wall-resolved large eddy simulation (WRLES) provide highly accurate solutions, their computational cost makes them prohibitively expensive for many engineering applications. In contrast, Reynolds-averaged Navier–Stokes (RANS) modeling is computationally less expensive and widely used in industry, especially when considering optimization problems or uncertainty quantification that both require a large number of simulations to explore a large parameter space. However, the accuracy of RANS simulations depends on the turbulence models used. Fig. 8.1 illustrates typical applications in which RANS models are commonly employed for flow simulations.

The modeling equations are commonly obtained by applying some form of averaging or filtering to the governing equations of fluid motion. In RANS, the flow field is decomposed into its mean and fluctuating parts, where the mean flow can be obtained for a statistically steady or homogeneous flow by averaging in time or space, respectively. In LES, the averaging is performed by applying a spatial filtering operator. Yet, in both approaches, due to the nonlinear nature of the compressible Navier–Stokes equations, additional terms appear in the governing equations that require closure. Therefore, turbulence modeling, particularly in the form of RANS model closures, remains critical for engineering design and optimization, where a balance between computational cost and accuracy is essential.

The development of RANS models has spanned over a century, starting with the pioneering work of Reynolds, Boussinesq, Prandtl, Kármán, and many others, who laid the foundation for understanding the effects of turbulent mixing. From the beginning, turbulence has been modeled through the use of simple algebraic equations. As computers became more prevalent, more complex models were developed, including transport equations for the eddy viscosity, two-equation models like the $k-\varepsilon$ and $k-\omega$ models, and models that solve all components of the Reynolds stress tensor, also called second-moment closure models.

Turbulence and Transition in Supersonic and Hypersonic Flows
https://doi.org/10.1016/B978-0-44-318785-8.00016-X

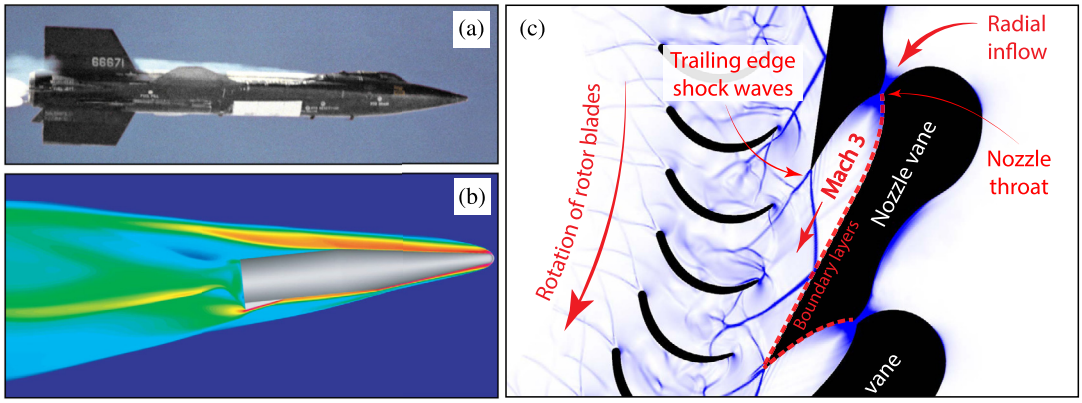

FIGURE 8.1 **Examples.** Visualizations of supersonic and hypersonic flows: (a) the NASA X-15, (b) a generic lifting hypersonic body, and (c) a RANS simulation of a radial inflow turbine operating with an organic fluid at Mach 3. Fig. (a) and (b) from Candler (2019), Fig. (c) adapted from Otero-Rodriguez et al. (2021).

The intent of this chapter is not to provide a comprehensive summary of RANS models and their developments. Instead, this chapter focuses on efforts to model compressible flows by highlighting how models that have been developed for incompressible flows can be adapted to account for fluid compressibility. We will limit the discussion to fully developed turbulent channel flows, highlighting how variable-property and intrinsic compressibility effects influence turbulence and how these effects can be modeled. The insights can be extended to more general wall-bounded flows in engineering applications.

In addition, we will contrast recent advancements in turbulence modeling with earlier approaches. Distinct direct numerical simulations (DNS) are discussed to separately examine variable-property and intrinsic compressibility effects, providing clear insights into their individual roles. Building on these insights, various modeling strategies are discussed in detail. The objective is to present a unified perspective on the progress in this field. Other modeling challenges, such as the treatment of shock waves and compressibility in free shear layers, are beyond the scope of this chapter. Additionally, machine learning techniques, which are currently an active area of research, are not discussed here.

Readers can replicate most of the results presented here using the Jupyter-Notebooks available on GitHub (Pecnik et al., 2023; Hasan and Pecnik, 2024; Pecnik and Hasan, 2023).

8.2 Governing equations

Before discussing closure models for compressible flows, the conservation equations of mass, momentum, and energy will be summarized. For these, several approximations will be used, not only to obtain a simplified set of equations but also to focus on modeling the main effects of compressibility. These approximations are:

- The fluid can be approximated with the ideal-gas equation of state to establish the relationship between density, temperature, and pressure.

- The analysis will further constrain to calorically perfect gases in which the specific heat capacities are constant. As a result, the caloric equation of state that relates the internal energy of the fluid with the thermodynamic state linearly depends on temperature.
- Unless otherwise stated, the dynamic viscosity is described by either a power law or Sutherland's law.
- Following Stokes's hypothesis, the bulk (volume) viscosity will be neglected. For work regarding non-zero bulk viscosity, refer to e.g., Pan and Johnsen (2017); Touber (2019).
- The fluid is limited to simple compressible substances, single phase, with no chemical reactions.
- Additional source terms, such as buoyancy, are not accounted for.

The simplified conservation equations for mass, momentum, and total energy are then given as

$$\frac{\partial \rho}{\partial t} + \frac{\partial \left(\rho u_j\right)}{\partial x_j} = 0, \tag{8.1}$$

$$\frac{\partial \left(\rho u_i\right)}{\partial t} + \frac{\partial \left(\rho u_i u_j\right)}{\partial x_j} = -\frac{\partial p}{\partial x_i} + \frac{\partial \tau_{ij}}{\partial x_j}, \tag{8.2}$$

$$\frac{\partial \left(\rho E\right)}{\partial t} + \frac{\partial \left(\rho u_j H\right)}{\partial x_j} = -\frac{\partial q_j}{\partial x_j} + \frac{\partial \left(u_i \tau_{ij}\right)}{\partial x_j}, \tag{8.3}$$

where the specific total energy is the sum of specific internal, e.g., and kinetic energy per unit mass, given as

$$E = e + \frac{u_i u_i}{2}, \tag{8.4}$$

and the specific total enthalpy is per definition

$$H = \underbrace{e + \frac{p}{\rho}}_{h} + \frac{u_i u_i}{2}. \tag{8.5}$$

With the caloric equation of state, the specific internal energy for an ideal gas is $e = c_v T$, with c_v the specific isochoric heat capacity. The specific enthalpy for an ideal gas is $h = c_p T$, with c_p the specific isobaric heat capacity. The ratio of the specific heat capacities is denoted by γ and is given by $\gamma = c_p / c_v$. The equation of state for an ideal gas relates pressure, density, and temperature as $p = \rho R T$, with R the specific gas constant.

The stress tensor τ_{ij} for a Newtonian fluid, neglecting the volume viscosity, is given by

$$\tau_{ij} = 2\mu S_{ij}, \tag{8.6}$$

with the deviatoric strain-rate tensor (constant volume deformation)

$$S_{ij} = \frac{1}{2}\left(\frac{\partial u_i}{\partial x_j} + \frac{\partial u_j}{\partial x_i}\right) - \frac{1}{3}\frac{\partial u_k}{\partial x_k}\delta_{ij}, \tag{8.7}$$

and μ the dynamic viscosity. The heat flux vector q_j is related to Fourier's law and is given by

$$q_j = -\lambda \frac{\partial T}{\partial x_j}, \tag{8.8}$$

with λ the thermal conductivity, often also expressed as

$$\lambda = \frac{c_p \mu}{Pr}, \tag{8.9}$$

with the Prandtl number Pr.

8.2.1 Reynolds and Favre averaging

The common approach in modeling compressible turbulent flows is to use a combination of Reynolds and Favre decomposition of the turbulent flow field. The textbooks of Friedrich (1999); Wilcox (2006); Smits and Dussauge (2006); Gatski and Bonnet (2013), provide a comprehensive summary of the most important averaging relations. To prevent redundancy, this section will focus only on the most essential relations that are required for the ensuing discussion.

The Reynolds decomposition for an arbitrary quantity f is defined as

$$f = \bar{f} + f', \tag{8.10}$$

with $\bar{f} = \bar{f}(\mathbf{x})$ the Reynolds average of a statistically steady or stationary turbulent field, and $f' = f'(\mathbf{x}, t)$ the fluctuation around that mean. Note that the Reynolds average of the fluctuating part is

$$\overline{f'} = 0. \tag{8.11}$$

Applying the Reynolds decomposition and successive averaging to the governing equations results in the appearance of several additional correlations. This can be demonstrated by Reynolds averaging the mass-conservation equation, which leads for a steady flow to

$$\frac{\partial}{\partial x_j}\left(\bar{\rho}\bar{u}_j + \overline{\rho' u'_j}\right) = 0. \tag{8.12}$$

The additional correlation $\overline{\rho' u'_j}$ complicates the modeling of turbulent compressible flows.

To simplify the equations, Favre introduced a density-weighted average in their studies of atmospheric flows (Favre, 1969). The density-weighted average is defined as

$$\widetilde{f} = \frac{\overline{\rho f}}{\bar{\rho}}, \tag{8.13}$$

such that the Favre decomposition can be written as

$$f = \widetilde{f} + f'', \tag{8.14}$$

with f'' the Favre fluctuating part of an instantaneous quantity f. In order to show how Favre averaging simplifies the final averaged equations, it is useful to derive two primary identities. Multiplying Eqs. (8.10) and (8.14) by the density ρ and then Reynolds averaging yields

$$\overline{\rho f} = \bar{\rho}\bar{f} + \overline{\rho' f'}, \tag{8.15}$$

$$\overline{\rho f} = \bar{\rho}\widetilde{f} + \overline{\rho f''}. \tag{8.16}$$

Reynolds averaging Eq. (8.14) and combining it with Eqs. (8.15) and (8.13) leads to the first identity that $\overline{f''}$ is non-zero, namely,

$$\widetilde{f} - \bar{f} = \frac{\overline{\rho' f'}}{\bar{\rho}} = -\overline{f''} \neq 0. \tag{8.17}$$

This is contrary to $\overline{f'}$, which is zero by definition. On the other hand, using Eq. (8.16), and again with the definition (8.13), it can be shown that

$$\overline{\rho f''} = 0, \tag{8.18}$$

which is the main reason why the averaged conservation equations are simpler when Favre averaging is employed for velocity, enthalpy, internal energy, and temperature.

8.2.2 Reynolds-averaged Navier–Stokes equations

Applying Reynolds decomposition for density, pressure, and viscous stress, and Favre decomposition for the remaining quantities, and then Reynolds averaging the conservation equations, yields the exact Reynolds-averaged Navier–Stokes equations

$$\frac{\partial\left(\bar{\rho}\widetilde{u}_j\right)}{\partial x_j} = 0, \tag{8.19}$$

$$\frac{\partial\left(\bar{\rho}\widetilde{u}_i\widetilde{u}_j\right)}{\partial x_j} = -\frac{\partial \bar{p}}{\partial x_i} + \frac{\partial \bar{\tau}_{ij}}{\partial x_j} - \frac{\partial\left(\widetilde{\bar{\rho}u_i''u_j''}\right)}{\partial x_j}, \tag{8.20}$$

$$\begin{aligned}\frac{\partial\left(\bar{\rho}\widetilde{u}_j\widetilde{H}\right)}{\partial x_j} &= -\frac{\partial \bar{q}_j}{\partial x_j} + \frac{\partial\left(\widetilde{u}_i\bar{\tau}_{ij}\right)}{\partial x_j} \\ &\quad - \frac{\partial}{\partial x_j}\left(\widetilde{u}_i\widetilde{\bar{\rho}u_i''u_j''} - \overline{u_i''\tau_{ij}} + \frac{1}{2}\widetilde{\bar{\rho}u_j''u_i''u_i''} + \widetilde{\bar{\rho}u_j''h''}\right).\end{aligned} \tag{8.21}$$

Eqs. (8.19)–(8.21) constitute conservation equations for Reynolds/Favre averaged mass, momentum, and specific total energy. Due to the averaging procedure, the Favre averaged specific total energy, $\widetilde{E}$, now also includes the turbulent kinetic energy per unit mass. It is defined as

$$\widetilde{E} = \widetilde{e} + \underbrace{\frac{1}{2}\widetilde{u}_i\widetilde{u}_i}_{\text{MKE}} + \underbrace{\frac{1}{2}\widetilde{u_i''u_i''}}_{\text{TKE, } k}, \tag{8.22}$$

where MKE is the mean and TKE is the turbulent kinetic energy, defined as

$$k = \frac{\widetilde{u_i'' u_i''}}{2}. \tag{8.23}$$

Equivalently, the Favre averaged total enthalpy, which appears in the advection term of the energy equation (8.21), is defined as

$$\widetilde{H} = \widetilde{h} + \mathrm{MKE} + \mathrm{TKE}. \tag{8.24}$$

It is worth noting that the turbulent kinetic energy is a small fraction of the total energy and is hence often neglected in RANS simulations. Although this simplification is useful in many cases, it is crucial to recognize that, in hypersonic boundary layers, k may contribute considerably to the total energy. For instance, for an ideal gas, it is possible to show that

$$\frac{k}{e} = \frac{\gamma(\gamma-1)}{2} M_t^2, \tag{8.25}$$

with the turbulent Mach number $M_t = \sqrt{2k}/a$, and a the speed of sound. For wall-cooled boundary layers at freestream Mach numbers of 14, k/e can reach values up to 0.15 (Zhang et al., 2018). In that case, k should not be neglected when computing pressure or temperature form the total energy in a CFD solver.

The definition of the enthalpy and the equation of state remain unchanged, but they are evaluated with the Reynolds-averaged pressure and density, and Favre averaged enthalpy, internal energy, and temperature, given as

$$\widetilde{h} = \widetilde{e} + \bar{p}/\bar{\rho}, \tag{8.26}$$

$$\bar{p} = \bar{\rho} R \widetilde{T}. \tag{8.27}$$

8.2.2.1 *Common approximations and preliminary models*

Compared to the instantaneous Navier–Stokes equations, additional correlations appear in the RANS equations that must be **approximated** or **modeled** to obtain a closed set of equations. The standard practice involves individually examining each of the terms. For completeness, we briefly summarize the most important ones.

Approximating the averaged stress tensor and heat flux vector. The first term that needs an approximation in the momentum equation (8.20) is the Reynolds-averaged stress tensor. It can be expanded as

$$\bar{\tau}_{ij} = 2\left(\bar{\mu}\bar{S}_{ij} + \overline{\mu' S'_{ij}}\right). \tag{8.28}$$

Eq. (8.28) now already reveals several modeling challenges while attempting to derive a closed form of the Navier–Stokes equation. First, the nonlinear functional relation for the dynamic viscosity generates a closure problem since $\bar{\mu} = \bar{f}(T, p) \neq f(\bar{T}, \bar{p})$. In other words this means that $\bar{\mu}$ can only be approximated with the averaged temperature and pressure and not calculated exactly if the functional relation $\mu = f(T, p)$ is highly nonlinear. Additionally,

the correlation $\overline{\mu' S'_{ij}}$ is unknown. Moreover, to compute $\bar{S}_{ij}$ the Reynolds-averaged velocity $\bar{u}_i$ is required, but $\bar{u}_i$ is unknown as well since the RANS equations are solving for $\widetilde{u}_i$.

To arrive at a practical solution for RANS simulations, it is necessary to introduce a few assumptions. Rewriting Eq. (8.28) by employing the Favre decomposition for the strain rate tensor, it is possible to obtain

$$\bar{\tau}_{ij} = 2\left[\bar{\mu}\left(\widetilde{S}_{ij} + \overline{S''_{ij}}\right) + \overline{\mu' S_{ij}}\right] \approx 2\bar{\mu}\widetilde{S}_{ij}, \tag{8.29}$$

with the assumptions that $\bar{\mu} \approx f(\widetilde{T}, \bar{p})$, that $\overline{S''_{ij}} \ll \widetilde{S}_{ij}$ and that the last term containing viscosity fluctuations is negligible. In the context of isothermal supersonic channel flows at Mach 4 with ideal gases, the error of this approximation is at most 2%. However, in flows at higher Mach numbers or in flows involving highly non-ideal gases such as supercritical fluids (Kawai, 2019), the error may be considerably higher (Fig. 7.7a).

Similarly, equivalent assumptions must be made regarding the Reynolds-averaged heat-flux vector, which is then approximated as

$$\bar{q}_i \approx \bar{\lambda}\frac{\partial \widetilde{T}}{\partial x_i} \approx \frac{\bar{c}_p \bar{\mu}}{Pr}\frac{\partial \widetilde{T}}{\partial x_i}. \tag{8.30}$$

For a more detailed discussion on the validity of these assumptions for high-speed flows with ideal gases, the reader is referred to Gatski and Bonnet (2013) (Chap. 3.3, page 54) and to Fig. 7.7(d).

Modeling the turbulent stress and heat flux. The next term that needs approximation in the momentum equation (8.20) is the Reynolds stress tensor $\bar{\rho}\widetilde{u''_i u''_j}$. Together with the turbulent heat flux vector $\bar{\rho}\widetilde{u''_j h''}$ (last term in (8.21)), they form the most critical correlations in turbulence modeling. The Reynolds stress tensor describes the momentum transfer, while the turbulent heat flux describes the heat transfer caused by turbulent mixing. Accurately modeling these correlations is vital in predicting the mean-flow field of turbulent flows.

The calculation of the Reynolds stress tensor can be approached in various manners. One method concerns deriving exact transport equations for each individual component of the Reynolds stress. Yet, these transport equations contain source terms that themselves consist of higher-order correlations. These higher-order correlations are unclosed, which means they lack a definitive expression and must be approximated or modeled in some way. This presents a significant challenge in turbulence modeling and is often referred to as the "closure problem in turbulence".

The by far most common approach in engineering is to assume that the turbulent momentum transport can be modeled analogously to the viscous momentum transport, known as the Boussinesq approximation. It is given as

$$-\bar{\rho}\widetilde{u''_i u''_j} = 2\mu_t \widetilde{S}_{ij} - \frac{2}{3}\bar{\rho}k\delta_{ij}, \tag{8.31}$$

with k the turbulent kinetic energy per unit mass and μ_t the eddy viscosity. This essentially means that the number of unknowns has been reduced to k and μ_t. Similarly, the turbulent

heat flux can be modeled as

$$\widetilde{\bar{\rho}u_j''h''} = -\frac{\mu_t}{Pr_t}\frac{\partial \widetilde{h}}{\partial x_j} = -\frac{\bar{c}_p\mu_t}{Pr_t}\frac{\partial \widetilde{T}}{\partial x_j}, \tag{8.32}$$

with the turbulent Prandtl number Pr_t, the turbulent Prandtl number defined as

$$Pr_t = \frac{\widetilde{u''v''}d\widetilde{T}/dy}{\widetilde{v''T''}d\widetilde{u}/dy}. \tag{8.33}$$

For air in the ideal gas regime, Pr_t is commonly assumed to be the range 0.9–1.0. A short discussion on this approximation is given in section 8.6.

Approximating and modeling the remaining terms in the energy equation. The remaining three unclosed correlations in the total energy equation are the work done on the fluid by the Reynolds stresses and the viscous diffusion and turbulent diffusion of turbulent kinetic energy. The first term, $\widetilde{u}_j\widetilde{\bar{\rho}u_i''u_j''}$, can be obtained once the Reynolds stress has been modeled. The second term, namely, the viscous diffusion, can be split into two parts, namely,

$$\overline{u_i''\tau_{ij}} = \overline{u_i''\left(\bar{\tau}_{ij} + \tau_{ij}'\right)} = \overline{u_i''}\bar{\tau}_{ij} + \overline{u_i'\tau_{ij}'}, \tag{8.34}$$

where the first term is a product of the turbulent mass flux $\overline{u_i''}$ and the Reynolds averaged stress tensor $\bar{\tau}_{ij}$. It is possible to derive an exact transport equation for $\overline{u_i''}$ (see Gatski and Bonnet (2013)) to gain insights into the physical processes. Based on these insights, models have been proposed by Rubesin (1990); Ristorcelli (1993); Zeman (1993). The model by Rubesin (1990) is given by

$$\overline{u_i''} = C_\rho\frac{k}{\varepsilon_M}\widetilde{u_i''u_j''}\frac{1}{\bar{\rho}}\frac{\partial\bar{\rho}}{\partial x_j}, \tag{8.35}$$

with C_ρ a parameter that is, unfortunately, not unique and depends on the individual component to be modeled in a wall-bounded flow (Huang et al., 1995). ε_M is the turbulent energy dissipation rate per unit mass (subscript M), namely, the amount of turbulent kinetic energy per unit mass that is dissipated per unit time (Joule/(kg·s)). It is important to note that in the compressible turbulent kinetic energy equation, the dissipation rate is typically defined on a per unit volume basis (Joule/(m^3·s)), which will be introduced later in Sect. 8.2.4. For modeling purposes, the relationship between the dissipation rate per unit volume and unit mass is simply given by

$$\varepsilon_V = \bar{\rho}\,\varepsilon_M. \tag{8.36}$$

This distinction should be kept in mind when modeling the dissipation rate for variable density flows. Most of the time, terms factored with the turbulent mass flux $\overline{u_i''}$ are, however, neglected in RANS simulations since their contributions are small (Wilcox, 2006).

The second term in Eq. (8.34) can be rewritten such that the turbulent kinetic energy appears. Neglecting viscosity fluctuations, the term can be approximated as (Friedrich, 1999)

$$\overline{u_i' \tau_{ij}'} \approx \bar{\mu} \left(\frac{\partial \overbrace{\frac{\overline{u_i' u_i'}}{2}}^{\approx k}}{\partial x_j} + \frac{\partial \overline{u_i' u_j'}}{\partial x_i} - \frac{5}{3} \overline{u_j' \frac{\partial u_i'}{\partial x_i}} \right). \tag{8.37}$$

When modeling wall-bounded flows, it can be shown that the gradient of the second and third term are small (Bradshaw and Perot, 1993), such that

$$\frac{\partial \overline{u_i' \tau_{ij}'}}{\partial x_j} \approx \frac{\partial}{\partial x_j} \left(\bar{\mu} \frac{\partial k}{\partial x_j} \right). \tag{8.38}$$

Finally, the turbulent diffusion of turbulent kinetic energy is approximated with the simple gradient diffusion hypothesis as

$$-\frac{1}{2} \bar{\rho} \widetilde{u_j'' u_i'' u_i''} = \frac{\mu_t}{\sigma_k} \frac{\partial k}{\partial x_j}, \tag{8.39}$$

where μ_t is the eddy viscosity and σ_k a modeling constant.

It is important to note that the approximations (8.38) and (8.39) also appear in the transport equation for the turbulent kinetic energy k. In Sect. 8.4.5 we will discuss how these approximations can be adapted to account for variable properties. These changes must then be carried over to the energy equation as well, which will be discussed in Sect. 8.6.

8.2.3 Final model RANS equations

After applying all these approximations and neglecting the terms with the turbulent mass flux $\overline{u_i''}$, the model RANS equations read

$$\frac{\partial \left(\bar{\rho} \widetilde{u}_j \right)}{\partial x_j} = 0, \tag{8.40}$$

$$\frac{\partial \left(\bar{\rho} \widetilde{u}_i \widetilde{u}_j \right)}{\partial x_j} = -\frac{\partial \bar{p}}{\partial x_i} + \frac{\partial}{\partial x_j} \left[2 \left(\bar{\mu} + \mu_t \right) \widetilde{S}_{ij} - \frac{2}{3} \bar{\rho} k \delta_{ij} \right], \tag{8.41}$$

$$\begin{aligned} \frac{\partial \left(\bar{\rho} \widetilde{u}_j \widetilde{H} \right)}{\partial x_j} = & \underbrace{\frac{\partial}{\partial x_j} \left[\bar{c}_p \left(\frac{\bar{\mu}}{Pr} + \frac{\mu_t}{Pr_t} \right) \frac{\partial \widetilde{T}}{\partial x_j} \right]}_{(1)} \\ & + \underbrace{\frac{\partial}{\partial x_j} \left[\widetilde{u}_i \left(2 \left(\bar{\mu} + \mu_t \right) \widetilde{S}_{ij} - \frac{2}{3} \bar{\rho} k \delta_{ij} \right) \right]}_{(2)} \end{aligned}$$

$$+\underbrace{\frac{\partial}{\partial x_j}\left[\left(\bar{\mu}+\frac{\mu_t}{\sigma_k}\right)\frac{\partial k}{\partial x_j}\right]}_{(3)}, \tag{8.42}$$

where the right-hand side of the total energy equation contains **molecular and turbulent diffusion** of (1) **mean internal**, (2) **mean kinetic**, and (3) **turbulent kinetic energies**, which is analogous to the constituents of the Favre-averaged total energy as given in Eq. (8.22).

The challenge of turbulence modeling has consequently been reduced to a mere handful of unknowns. Specifically, the remaining unknowns in the RANS equations just listed are μ_t and k, along with a small number of constants such as Pr_t and σ_k. It is important to remember that this represents a significant simplification that is prone to failure in several specific situations. In particular, the Boussinesq approximation, which is also applied for incompressible flows, has several shortcomings that have been discussed in detail in Pope (2000); Pettersson Reif and Durbin (2011).

8.2.4 Turbulent kinetic energy equation

The challenge is now to obtain the eddy viscosity and the turbulent kinetic energy. We first proceed by stating the exact transport equation for the turbulent kinetic energy that serves as a physics-based foundation for formulating the most common turbulence models. Two-equation models, such as $k-\varepsilon$ or the $k-\omega$, directly incorporate this equation (with certain modeling approximations) to account for the transport of TKE. Ultimately, the TKE together with the (specific) turbulent dissipation or turbulent length scale is used to estimate the eddy viscosity.

The transport equation for the turbulent kinetic energy can be derived by multiplying the momentum equation by the velocity fluctuations and then Reynolds averaging the result. A term-by-term derivation for compressible flows is given in Wilcox (2006). The main focus here is to highlight a few key concepts that play a crucial role in modeling the TKE for compressible flows. The transport equation for the turbulent kinetic energy is given by

$$\frac{\partial \bar{\rho} k}{\partial t}+\frac{\partial \bar{\rho}\,\widetilde{u}_j k}{\partial x_j}=P-\varepsilon_V+T+\Pi_d-F, \tag{8.43}$$

with the terms on the right-hand side representing the production of turbulent kinetic energy

$$P=-\bar{\rho}\widetilde{u_i''u_j''}\frac{\partial \widetilde{u}_i}{\partial x_j}, \tag{8.44}$$

turbulent dissipation rate per unit volume (subscript V)

$$\varepsilon_V=\overline{\tau_{ij}'\frac{\partial u_i'}{\partial x_j}}, \tag{8.45}$$

transport (containing in order of appearance: viscous diffusion, turbulent transport, and pressure diffusion)

$$T=\frac{\partial}{\partial x_j}\left(\overline{u_i'\tau_{ij}'}-\bar{\rho}\frac{1}{2}\widetilde{u_j''u_i''u_i''}-\overline{p'u_j'}\right), \tag{8.46}$$

pressure–dilatation correlation

$$\Pi_d = \overline{p' \frac{\partial u_i'}{\partial x_i}}, \tag{8.47}$$

and terms multiplied by the turbulent mass flux

$$F = \overline{u_i''} \left(\frac{\partial \bar{p}}{\partial x_i} - \frac{\partial \bar{\tau}_{ij}}{\partial x_j} \right). \tag{8.48}$$

8.2.4.1 *Preliminary modeling approximations for the TKE*

The TKE equation has three new unclosed terms, which are the dissipation rate ε_V, the pressure diffusion $\partial \overline{p' u_j'} / \partial x_j$ in (8.46), and the pressure–dilatation correlation Π_d. The other correlations, such as turbulent mass flux $\overline{u_i''}$, turbulent transport $\widetilde{u_j'' u_i'' u_i''}/2$, and viscous diffusion $\overline{u_i' \tau_{ij}'}$, have already been discussed as part of the modeling assumptions in Sect. 8.2.2.1; more specifically Eqs. (8.35), (8.38) and (8.39), respectively. Given that the Boussinesq approximation, Eq. (8.31), is employed, the production of TKE can also be evaluated and is thus known.

The transport equation for the dissipation rate relies heavily on empirical arguments. Its mathematical form is similar to the TKE conservation equation and includes several model coefficients that are determined based on experimental or DNS data for incompressible flows. For compressible flows, the dissipation rate (per unit mass or per unit volume) can be split into a solenoidal and a dilatational part (Zeman, 1990; Sarkar et al., 1991), usually written as

$$\varepsilon = \varepsilon_s + \varepsilon_d = \varepsilon_s \left(1 + \frac{\varepsilon_d}{\varepsilon_s} \right). \tag{8.49}$$

The standard incompressible model for turbulent dissipation is used to obtain ε_s, which is said to be unaffected by compressibility effects (Huang et al., 1995). The compressibility effects are then accounted for through the dilatational dissipation rate, which is commonly modeled as function of turbulent Mach number M_t, namely,

$$\varepsilon_d \propto f(M_t)\, \varepsilon_s. \tag{8.50}$$

Blaisdell et al. (1993) found that the ratio in homogeneous shear flows can be up to 20% and that it can be modeled proportional to M_t^2. In contrast, for compressible wall-bounded flows, (Huang et al., 1995) showed that the ratio is not correlated with M_t and that its magnitude is in the order of only 0.1% for a compressible channel flow at a bulk Mach number of 3. Zhang et al. (2018) showed that the ratio is small ($< 6\%$) everywhere for their boundary layer cases up to freestream Mach numbers of 8, and becomes non-negligible ($\approx 10\%$) only very close to the wall at a Mach number of 14. Moreover, dilatational dissipation is also found to be insignificant in mixing layers (Vreman et al., 1996). Yet, their models are often used to improve RANS predictions for compressible mixing layers and boundary-layer flows, albeit for the wrong reasons (Rumsey, 2010). Various models for dilatational dissipation are discussed in Sect. 8.5.

Similar conclusions can be made for the pressure–dilatation correlation Π_d. The pressure–dilatation correlation appears to be negligible for boundary layers up to Mach number of 14 (Zhang et al., 2018), except in the viscous sublayer ($y^\star < 5$) due to high dilatation magnitude in that region. Also, the correlation is not found to be significant in mixing layers (Vreman et al., 1996). Hence, no models are required as such, however, some commonly proposed models that improve results, again for the wrong reasons, are discussed in Sect. 8.5.

The pressure diffusion $\partial \overline{p' u_j'}/\partial x_j$ is commonly lumped together with the turbulent transport and modeled with the gradient diffusion hypothesis as given by Eq. (8.39).

The final turbulent kinetic energy equation with the approximations and models is given as

$$\frac{\partial \bar{\rho} k}{\partial t} + \frac{\partial \bar{\rho}\, \widetilde{u}_j k}{\partial x_j} = P - \varepsilon_V + \underbrace{\frac{\partial}{\partial x_j}\left[\left(\bar{\mu} + \frac{\mu_t}{\sigma_k}\right)\frac{\partial k}{\partial x_j}\right]}_{\text{same as (3) in Eq. (8.42)}} + \Pi_d - F, \tag{8.51}$$

with

$$P = \left(2\mu_t \widetilde{S}_{ij} - \frac{2}{3}\bar{\rho} k \delta_{ij}\right)\frac{\partial \widetilde{u}_i}{\partial x_j}. \tag{8.52}$$

8.3 Modeling classification of compressible flows

In the previous section, we discussed the additional terms that arise in the RANS and the TKE equations and summarized some of most common models for these terms. However, we noted that these models do not accurately capture the underlying physics, particularly in wall-bounded flows, where effects like pressure dilatation, dilatational dissipation, and turbulent mass flux are small. Despite this, the conventional models are quite inaccurate for compressible boundary-layer flows. So, what needs improvement?

To improve these models, we must first understand the specific effects present in high-speed wall-bounded flows. Only then can we adapt turbulence models to accurately reflect the turbulence dynamics. The two most important effects to consider are

- **Heat transfer** causing changes in thermophysical properties, such as density and viscosity; also called variable-property effects.
- **Intrinsic compressibility** resulting in density variations in response to pressure fluctuations.

It is critical that compressibility corrections—defined as the modifications that one needs to make to adapt a turbulence model for compressible flows—account for these two distinct mechanisms and remain consistent with the underlying physics, whether dealing with heat transfer (variable-property effects) or intrinsic compressibility.

Fig. 8.2 illustrates these effects in a high-speed turbulent boundary-layer flow that is cooled at the wall. Heat transfer induces property variations, while, at high flow speeds, intrinsic compressibility effects also become significant, where strong pressure fluctuations lead to density changes. Both effects are discussed in detail in the following.

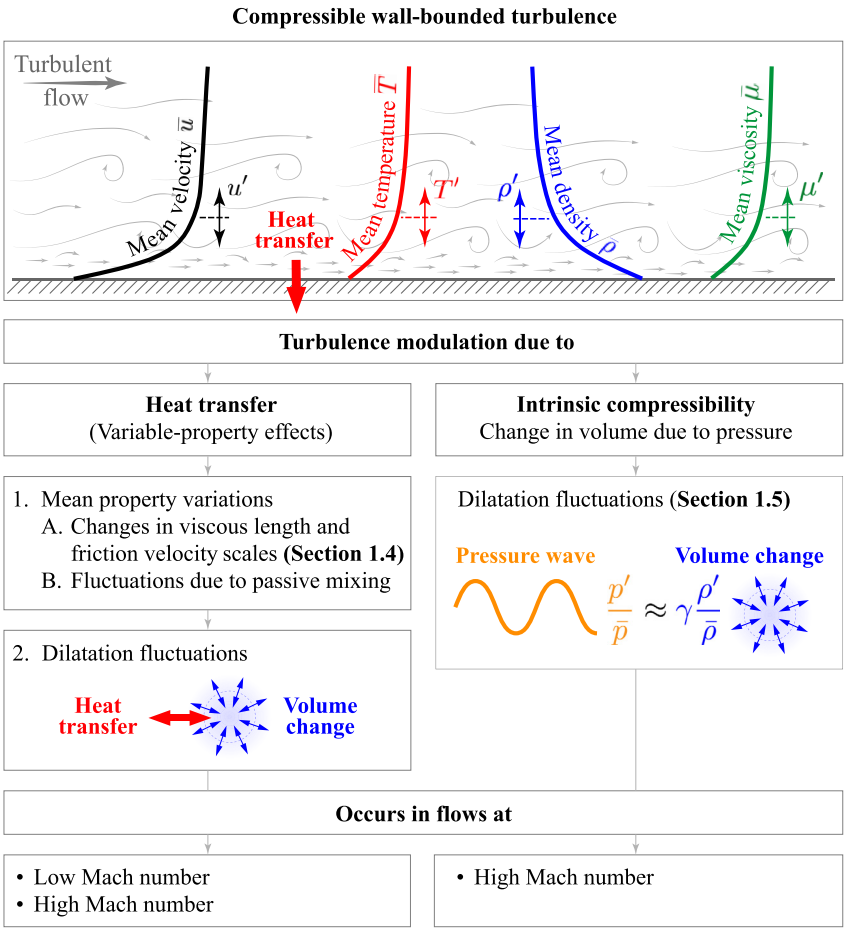

FIGURE 8.2 Schematic overview of the compressibility effects in wall-bounded turbulence. The diagram delineates two primary mechanisms: 1) heat transfer leading to changes in fluid properties, subdivided into mean variations and fluctuations due to mixing, and fluctuations in dilatation, and 2) isentropic changes in fluid volume induced by pressure fluctuations.

8.3.1 Heat transfer

Heat transfer modulates a turbulent boundary layer through two primary mechanisms (see left-hand column in Fig. 8.2): (1.) mean property variations, leading to (1.A.) changes in viscous length and friction velocity scales, and (1.B.) turbulent mixing across gradients. At small scales, if a turbulent eddy is surrounded by a hotter or colder fluid, heat transfer can cause a local expansion or contraction, which then modulates turbulence dynamics through (2.) dilatation fluctuations. These effects are present in both strongly heated or cooled flows at low Mach numbers and in high Mach-number flow, where significant viscous dissipation leads to large changes in temperature.

Related to mean property variations, changes in density alone give rise to what is known as variable inertia effects, which manifest as fluid parcels with different densities react differently to imposed pressure forces. These inertial effects can cause substantial asymmetries in mixing, turbulence, and the shape of mixing layers due to the influence of inertial baroclinic torque (Livescu, 2020). Besides this, density variations, along with mean viscosity variations, modify the viscous length and friction velocity scales in turbulent flows. Similarly, changes in thermal conductivity and specific heat capacities influence the turbulent temperature field. How these changes–induced by heat transfer—affect turbulence and how they can be accounted for in modeling turbulence is the topic of Sect. 8.4. Moreover, mean gradients in properties also cause fluctuations in properties due to passive mixing, affecting turbulence.

Dilatation due to heat transfer can be understood by rewriting the continuity equation

$$-\frac{1}{\rho}\frac{D\rho}{Dt} = \frac{1}{v}\frac{Dv}{Dt} = \frac{\partial u_i}{\partial x_i}, \tag{8.53}$$

to obtain a relation between density and dilatation, $\partial u_i/\partial x_i$. In the previous equation, the specific volume is $v = 1/\rho$, and D indicates the material derivative. Expressing the total derivative of density as a function of partial derivatives of entropy and pressure, it is possible to obtain a governing equation for the dilatation of a compressible substance at the low Mach number limits as

$$\frac{\partial u_i}{\partial x_i} = -\frac{1}{\gamma P_0}\frac{dP_0}{dt} - \frac{R}{c_p P_0}\left[\Phi - \frac{\partial q_i}{\partial x_i}\right], \tag{8.54}$$

where the background (thermodynamic) pressure, P_0, is uniform in space, and Φ is an arbitrary source term corresponding to a heat source arising from reactions, radiation, or other types of volumetric heating. Hence, dilatation can occur due to changes in background pressure P_0 (e.g., a closed system undergoing volume change or heat transfer), local heat transfer q, and heating or cooling by a local source Φ.

In low-speed flows, these effects can be rigorously analyzed using DNS with the low Mach-number approximation of the Navier–Stokes equations (Majda and Sethian, 1985). This approximation decomposes the pressure into hydrodynamic and thermodynamic components whose ratio is in the order of a reference Mach number squared. As a result, when the Mach number is small, thermodynamic density fluctuations are decoupled from hydrodynamic pressure fluctuations. In other words, the gas cannot undergo isentropic (reversible) compression or expansion. As a result, the low Mach-number approximation also does not contain any acoustic waves that propagate within the domain. This approach is thus the preferred choice to study how heat transfer affects turbulence to consequently develop turbulence models that account for these effects.

8.3.2 Intrinsic compressibility effects

The term intrinsic compressibility effect refers to the mechanism when density variations in a turbulent flow are induced by pressure fluctuations (see right-hand column in Fig. 8.2). Lele (1994) states "The importance of separating compressibility effects from effects of variable inertia cannot be overemphasized."

Kovasznay (1953) proposed a decomposition that separates a compressible turbulent flow field into vorticity, acoustic, and entropy modes for weakly compressible linear problems, where intrinsic compressibility effects are associated with the acoustic mode. Strictly speaking, this decomposition is limited to isotropic compressible turbulence. In non-homogeneous flows, the Helmholtz decomposition can be used that separates the velocity field into solenoidal and compressible modes. The latter, associated with intrinsic compressibility effects, is mainly caused by dilatation as a consequence of pressure given as

$$\frac{\partial u_i}{\partial x_i} \approx -\frac{1}{\gamma p}\frac{Dp}{Dt}. \tag{8.55}$$

Significant progress has been recently made in analyzing intrinsic compressibility effects for wall-bounded flows. Yu et al. (2019) observed that the near-wall dilatation motions are dynamically significant and counteract wall-ward sweep motions, affecting wall-shear stress by 10%. Similar observations were made in Yu and Xu (2021). However, in their DNS cases, both variable-property effects and intrinsic compressibility effects were present. This complicates the effort to differentiate between these effects since the distinction between them gets blurred (Lele, 1994).

To better assess the importance of intrinsic compressibility effects in wall-bounded flows, one can perform DNS of high Mach-number flows with nearly uniform mean properties. This approach was suggested by Coleman et al. (1995), who removed the viscous heating term in the energy equation. Such DNS results in a flowfield with nearly uniform mean temperature and thus properties in the entire domain, thereby effectively removing the impact of variable-property effects. Their findings confirmed Morkovin's hypothesis, which states that, at non-hypersonic Mach numbers, intrinsic compressibility effects are small and only mean property variations remain important for turbulence modeling.

In contrast, a subsequent study by Hasan et al. (2025a), using the same approach but at bulk Mach numbers up to 4, found that intrinsic compressibility effects are significant and cannot be ignored when modeling turbulence dynamics in wall-bounded high Mach-number flows. The study revealed that near the wall, the high rate of change in pressure produces large dilatation fluctuations with opposing sign. This dilatation leads to a substantial wall-normal dilatational velocity that opposes sweeps and ejections. This opposition weakens streamwise vortices, which in turn reduces the energy transfer from the streamwise velocity component to the other two velocity components. This weakening causes a reduction in the wall-normal turbulent stress as Mach number increases. Since wall-normal motions are critical in transporting momentum across the mean shear, the reduction in wall-normal turbulent stress also reduces the turbulent shear stress. The modeling of this effect is topic of Sect. 8.5.

8.4 Modeling variable-property effects

Now that we have distinguished between heat transfer and intrinsic compressibility effects, we can focus on modeling heat transfer-related effects. The key ingredient here is to properly account for mean variations in thermophysical properties. As we will outline in the

next section, this involves more than simply expressing density, viscosity, and other properties as functions of temperature and pressure in the governing equations.

Perhaps the most effective approach to sensitize turbulence models for mean property variations is to ensure that they are consistent with the semi-local scaling framework. Before we begin, we will introduce the definitions of both conventional and semi-local friction velocity and viscous length scales.

8.4.1 Definitions of viscous velocity and length scales

8.4.1.1 Conventional wall-based scaling

Wall scaling for constant-property flows utilizes reference values at the wall (subscript w) to define the friction velocity

$$u_\tau = \sqrt{\frac{\bar{\tau}_w}{\rho_w}}, \tag{8.56}$$

with $\bar{\tau}_w$ the averaged wall shear stress. The viscous length scale is defined as

$$\delta_v = \frac{\mu_w}{\rho_w u_\tau}. \tag{8.57}$$

The corresponding friction Reynolds number and dimensionless wall coordinate are then

$$Re_\tau = \frac{L}{\delta_v} = \frac{\rho_w u_\tau L}{\mu_w}, \tag{8.58}$$

and

$$y^+ = \frac{y}{\delta_v} = \left(\frac{y}{L}\right) Re_\tau, \tag{8.59}$$

where L is a reference length scale (channel half-height h or boundary-layer thickness δ). Additionally, the non-dimensional velocity is commonly defined as

$$u^+ = \frac{\bar{u}}{u_\tau}. \tag{8.60}$$

The mean velocity $\bar{u}^+$ for incompressible turbulent wall-bounded flows collapses as a function of the wall-normal distance y^+, independent of the Reynolds number. This is known as the law of the wall, which is one of the cornerstones of fluid dynamics (Bradshaw and Huang, 1995).

8.4.1.2 Semi-local scaling

For wall-bounded flows with changes in properties due to heat transfer, the friction velocity and length scales can be defined with locally averaged values of density and viscosity along the wall-normal direction (see Fig. 8.2), while the value of the shear stress is still taken at the wall. Hence, these scales are called "semi-local" scales and are defined as

$$u_\tau^\star = \sqrt{\frac{\bar{\tau}_w}{\bar{\rho}}}, \tag{8.61}$$

and

$$\delta_v^\star = \frac{\bar{\mu}}{\bar{\rho} u_\tau^\star}, \tag{8.62}$$

respectively. The corresponding semi-local friction Reynolds number can be related to the conventional friction Reynolds number as

$$Re_\tau^\star = \frac{L}{\delta_v^\star} = \frac{\bar{\rho} u_\tau^\star L}{\bar{\mu}} = \frac{\sqrt{\bar{\rho}/\bar{\rho}_w}}{\bar{\mu}/\bar{\mu}_w} Re_\tau. \tag{8.63}$$

Note that the density and viscosity at the wall are also averaged since they may fluctuate if they depend on pressure or if the wall is non-isothermal. The dimensionless wall coordinate is then obtained as

$$y^\star = \frac{y}{\delta_v^\star} = \left(\frac{y}{L}\right) Re_\tau^\star. \tag{8.64}$$

The concept of semi-local scaling dates back to Van Driest (1951) and Morkovin (1962), who proposed to scale the mean shear and the turbulent stresses by a velocity scale based on mean density, i.e., $u_\tau^\star$ (Hasan et al., 2025a). Later, Huang et al. (1995); Coleman et al. (1995) extended this local scaling approach to the viscous length scale. They showed that a good collapse of turbulent stresses at different Mach numbers is obtained when plotted as a function of wall distance scaled by the semi-local viscous length scale $\delta_v^\star$.

The scaling for the mean velocity is more intricate and there is not equivalent to Eq. (8.60). In other words, directly scaling the velocity of compressible wall-bounded flows by $u_\tau^\star$ and plotting it against the semi-local wall distance $y^\star$ fails to collapse compressible velocity profiles with the universal law of the wall of incompressible, constant-property flows. A more suitable velocity scaling methodology can be obtained by not only accounting for changes in the friction velocity scale, but also in changes of the viscous length scale. This will be discussed in more detail in the next section, as it is intimately linked to turbulence modeling.

8.4.2 Variable-property turbulent channel flows

The most effective approach to study variable-property effects is to consider DNS with the low Mach-number approximation of the Navier–Stokes equations. This method facilitates the distinction between variable-property effects and intrinsic compressibility effects. Similarly, Lele (1994) states "*One way to identify the variable inertia effects imbedded in compressible boundary layers is to contrast the high Mach number boundary layers with strongly heated, low-speed boundary layers*".

A valuable contribution by Patel et al. (2015) was to build on this idea to perform tailored simulations to study the effect of variable-properties on turbulence in channel flows at the zero Mach-number limit. They conducted DNS of turbulent channel flows with uniform volumetric heating, while maintaining a constant temperature at both channel walls such that temperature increases towards the channel center. By applying various temperature-dependent laws for density and viscosity, they explored a broad range of cases in which density, viscosity, or both, are varied, allowing them to isolate the individual effects of these variable properties on turbulence.

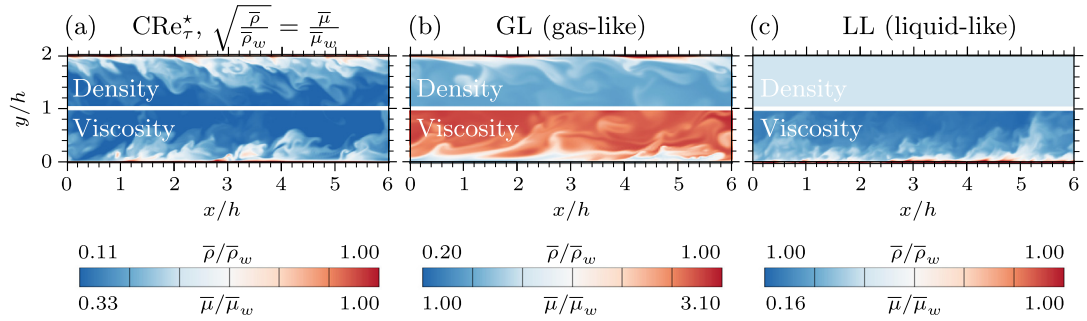

FIGURE 8.3 Contour plots of instantaneous density ρ (top half) and dynamic viscosity μ (lower half) for cases CRe$^\star_\tau$ (a), GL (b), and LL (c). The case GL exhibits a density change similar to an ideal gas flow at Mach 4 in a channel with isothermal walls. The values at the color scales indicate the maximum and minimum normalized values for density and viscosity. Adapted with permission from JFM, Pecnik and Patel (2017).

Fig. 8.3 displays some of the cases considered in their study. They employed various constitutive relations for density and viscosity as functions of temperature to mimic the thermodynamic behavior of air, water, and a fluid that is heated at supercritical pressure, particularly across the pseudo-boiling point where both density and dynamic viscosity rapidly decrease. The case of the supercritical fluid inspired them to find a fluid where both density and viscosity decrease. More specifically, a fluid for which the viscosity is proportional to the square root of density, such that the semi-local Reynolds number (Eq. (8.63)) remains constant throughout the channel. This case allows for a one-to-one comparison with a constant-property flow at the same semi-local friction Reynolds number.

They considered six cases that are organized into pairs of two, with each pair exhibiting a similar distribution of semi-local Reynolds numbers. These cases are shown in Fig. 8.4(a). The first two cases (indicated with black color) have a constant semi-local Reynolds number, with the first case having constant properties (case CP, with $Re_\tau = 395$, same as Moser et al. (1999)), while the second case has density and viscosity variations related by $\sqrt{\bar\rho/\bar\rho_w} = \bar\mu/\bar\mu_w$ (case CRe$^\star_\tau$). The second pair (indicated in red) consists of a case that resembles a liquid-like behavior (LL), and a case that shares a similar semi-local Reynolds-number distribution to case LL (named SRe$^\star_{\tau\mathrm{LL}}$), albeit with different density and viscosity distributions. Similarly, the third pair (indicated in blue) consists of a case that resembles a gas-like behavior (GL), and a case with similar Re$^\star_\tau$ distribution to case GL, named SRe$^\star_{\tau\mathrm{GL}}$. The given cases provide an optimal framework to study turbulence modification due to variable properties, without any effects caused by high Mach numbers.

Fig. 8.4(b) shows the Van Driest (1951) velocity profiles as a function of y^+. The Van Driest velocity transformation was proposed to account for mean density variations to collapse adiabatic high-speed boundary layer velocity profiles with the law of the wall of an incompressible, constant-property flow. This transformation is given as

$$\bar u^{\mathrm{vD}} = \int_0^{\bar u/u_\tau} \sqrt{\frac{\bar\rho}{\bar\rho_w}}\, d\left(\frac{\bar u}{u_\tau}\right), \tag{8.65}$$

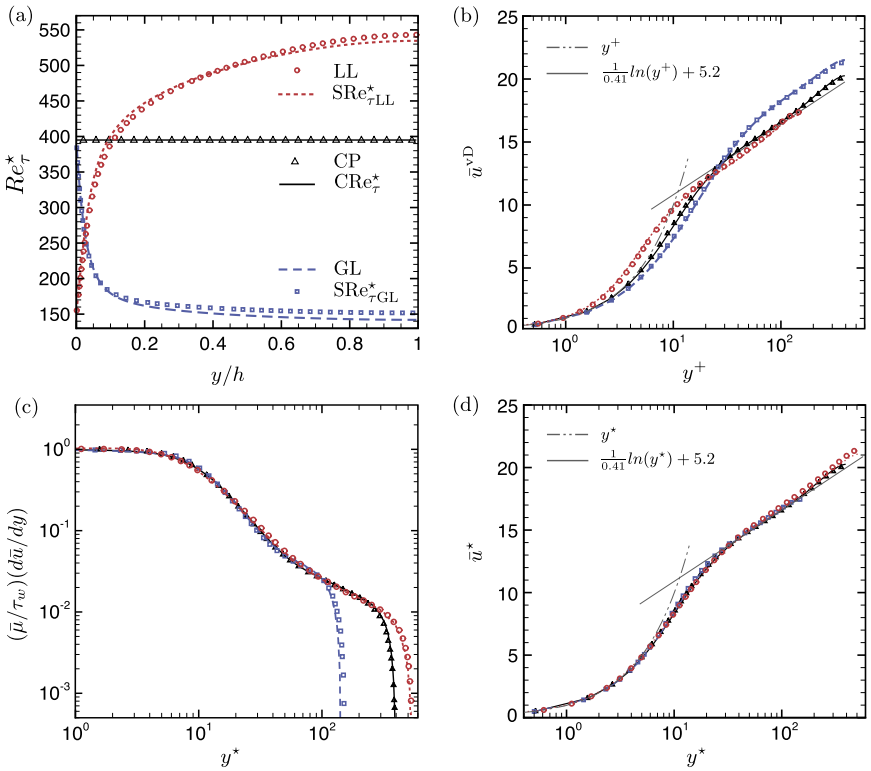

FIGURE 8.4 (a) Semi-local Reynolds number $Re^{\star}_{\tau}$, (b) van Driest velocity $\overline{u}^{\mathrm{vD}}$, (c) normalized viscous shear stress, and (d) semi-local velocity transformation $\bar{u}^{\star}$ for six cases that all have different mean densities and viscosity distributions. These cases are organized into three pairs, with each pair sharing similar semi-local Reynolds-number distributions.

or defining it in differential form as

$$d\bar{u}^{\mathrm{vD}} \equiv \sqrt{\frac{\bar{\rho}}{\bar{\rho}_w}} d\left(\frac{\bar{u}}{u_\tau}\right) = \frac{1}{u^{\star}_{\tau}} d\bar{u}. \tag{8.66}$$

In other words, the Van Driest velocity transformation accounts for variations in the friction velocity scale.

One important observation is that the $\bar{u}^{\mathrm{vD}}$ profiles are essentially the same for cases with similar $Re^{\star}_{\tau}$ distributions, or similar distributions of semi-local viscous length scale, since $\delta^{\star}_{v} = L/Re^{\star}_{\tau}$. In cases where density and viscosity vary such that $\delta^{\star}_{v}$ remains constant, the velocity profile essentially collapses with the incompressible law of the wall. This behavior is consistent with high-speed adiabatic boundary layers, for which $\delta^{\star}_{v}$ in the near-wall region remains nearly constant as well. However, in flows with gradients in $\delta^{\star}_{v}$—such as in heated, or cooled high-speed boundary layers or high-speed channel flows with isothermal walls—the $\bar{u}^{\mathrm{vD}}$ profiles do not collapse with the incompressible law of the wall. Although these

observations are based on simulations at the zero Mach-number limit, the same conclusions have been drawn from numerous DNS of supersonic channel, such as Coleman et al. (1995); Lechner et al. (2001); Foysi et al. (2004); Morinishi et al. (2004) and boundary-layer flows with heat transfer, such as Duan et al. (2010); Lagha et al. (2011); Shadloo et al. (2015); Modesti and Pirozzoli (2016).

The next observation is shown in Fig. 8.4(c). As seen, the viscous stresses, non-dimensionalized by the averaged wall shear stress $\bar{\tau}_w$,

$$\frac{\bar{\mu}}{\bar{\tau}_w}\frac{d\bar{u}}{dy} \tag{8.67}$$

nearly collapse for all cases in the inner layer when plotted as a function of $y^\star$. This observation is fundamental since it forms the basis for developing scaling laws for variable-property flows and, ultimately, turbulence models.

8.4.2.1 *Equivalence of mean shear in the inner layer*

Focusing on the viscous stress, its non-dimensional form can also be written using the definitions of the friction velocity and viscous length scale. For a **constant-property flow**, using $\tau_w = \rho_w u_\tau^2$ and $\mu_w = \rho_w u_\tau \delta_v$, the viscous stress is then

$$\frac{\mu_w}{\tau_w}\frac{d\bar{u}}{dy} = \frac{\rho_w u_\tau \delta_v}{\rho_w u_\tau^2}\frac{d\bar{u}}{dy} = \boxed{\frac{\delta_v}{u_\tau}\frac{d\bar{u}}{dy} = \frac{du^+}{dy^+}.} \tag{8.68}$$

Analogously, for a **variable-property flow**, using the definitions defined in section 8.4.1.2, we can write the viscous stress as

$$\frac{\bar{\mu}}{\tau_w}\frac{d\bar{u}}{dy} = \frac{\bar{\rho} u_\tau^\star \delta_v^\star}{\bar{\rho} u_\tau^{\star 2}}\frac{d\bar{u}}{dy} = \boxed{\frac{\delta_v^\star}{u_\tau^\star}\frac{d\bar{u}}{dy} = \frac{d\bar{u}^\star}{dy^\star}.} \tag{8.69}$$

The most important observation here is that the mean shear $d\bar{u}/dy$ is non-dimensionalized by the semi-local friction velocity and the semi-local viscous length scale. The last term in Eq. (8.69) is written as a direct analogy to $d\bar{u}^+/dy^+$. Since the viscous stresses for the variable-property collapse well in Fig. 8.4(c), this presentation of viscous stress makes the one-to-one correspondence between the constant- and variable-property formulations clear, which can be stated as follows:

$$\underbrace{\frac{du^+}{dy^+} = \frac{\delta_v}{u_\tau}\frac{d\bar{u}}{dy}}_{\text{constant-property}} \approx \underbrace{\frac{\delta_v^\star}{u_\tau^\star}\frac{d\bar{u}}{dy} = \frac{d\bar{u}^\star}{dy^\star}}_{\text{variable-property}}. \tag{8.70}$$

This is an important conclusion for two reasons. First, it shows that the shear $d\bar{u}/dy$, when scaled by the proper friction velocity and viscous length scale, is equivalent for constant- and variable-property flows. Secondly, it implies that the non-dimensional shear $d\bar{u}^\star/dy^\star$ can be used to derive the semi-locally scaled velocity transformation for variable-property flows.

Since the viscous stresses for all cases collapse well when they are plotted as a function of $y^\star$ (see Fig. 8.4(c)), we use the last two terms of Eq. (8.70) to form the basis for the velocity transformation, namely,

$$\bar{u}^\star = \int \left(\frac{\delta_v^\star}{u_\tau^\star} \frac{d\bar{u}}{dy} \right) dy^\star. \tag{8.71}$$

With the definition of $y^\star = y/\delta_v^\star$, see Eq. (8.64), we can further write

$$\bar{u}^\star = \int_0^{\bar{u}} \left(1 - \frac{y}{\delta_v^\star} \frac{d\delta_v^\star}{dy} \right) \underbrace{\frac{1}{u_\tau^\star} d\bar{u}}_{d\bar{u}^{\mathrm{vD}}}, \tag{8.72}$$

as written in Hasan et al. (2024). With the definition of the semi-local Reynolds number, it can also be written in the form as it was derived by Patel et al. (2016b) as

$$\bar{u}^\star = \int_0^{\bar{u}^+} \left(1 + \frac{y}{Re_\tau^\star} \frac{dRe_\tau^\star}{dy} \right) d\bar{u}^{\mathrm{vD}}. \tag{8.73}$$

The profiles for $\bar{u}^\star$ are shown in Fig. 8.4(d). As expected, the transformed velocity profiles for the variable-property cases collapse onto the incompressible, constant-property law of the wall, similar to the collapse observed for the viscous stresses in Fig. 8.4(c). Note that, when using the definition of $Re_\tau^\star$, it can be shown that this velocity transformation is mathematically equivalent to the transformation proposed by Trettel and Larsson (2016), who derived it on the basis of compressible, high Mach-number channel flows.

In the form just given, it is possible to recognize that, for small gradients of the semi-local viscous length scales, the transformation reduces to the van Driest velocity transformation. This is the reason why the van Driest velocity transformation works well for adiabatic high-speed flows where the near-wall viscous length scale, or semi-local Reynolds number, is almost constant. However, for flows with strong heat transfer, the van Driest velocity transformation fails to collapse the velocity profiles with the incompressible, constant-property law of the wall, while Eq. (8.72) accounts for changes in the viscous length scale for such flows. It is important to note that this transformation is expected to work well for flows where the stress balance holds—on which it is based—and when intrinsic compressibility effects are small, i.e., in flows at low Mach number. This transformation, especially the semi-locally scaled form of the shear, forms the basis for developing eddy viscosity models for wall-bounded variable-property flows, discussed next.

8.4.2.2 Equivalence of total stress in the inner layer

The total stress-balance relationship for the turbulent and viscous stresses can be obtained by integrating the mean streamwise momentum equation. The stress balance for quasi-parallel wall shear flows, non-dimensionalized by the wall shear stress τ_w, is given by

$$\frac{\bar{\mu}}{\bar{\tau}_w} \frac{d\bar{u}}{dy} - \frac{\widetilde{\bar{\rho} u'' v''}}{\bar{\tau}_w} \approx \frac{\bar{\tau}_t}{\bar{\tau}_w}, \tag{8.74}$$

where $\bar{\tau}_t$ and $\bar{\tau}_w$ are the total and wall shear stress, respectively. The approximate sign indicates that correlations with viscosity fluctuations have been neglected, namely, $\overline{\mu' S'_{ij}} \approx 0$. For boundary layer flows, $\bar{\tau}_t$ is approximately constant in the inner layer, while it varies linearly for channel flows as $\bar{\tau}_t/\bar{\tau}_w = 1 - y/H$.

Using the Boussinesq approximation (Eq. (8.31)), the Reynolds shear stress can be written as

$$-\bar{\rho}\widetilde{u''v''} = \mu_t \frac{d\widetilde{u}}{dy} \approx \mu_t \frac{d\bar{u}}{dy}. \tag{8.75}$$

Using the definitions of $u_\tau^\star$ and $\delta_v^\star$ and assuming the total shear stress to be universal, we can show the equivalence of the total stresses for constant- and variable-property flows, as

$$\underbrace{\left(1 + \frac{\mu_t}{\mu_w}\right)\frac{d\bar{u}^+}{dy^+}}_{\text{constant-propery}} \approx \underbrace{\left(1 + \frac{\mu_t}{\bar{\mu}}\right)\frac{d\bar{u}^\star}{dy^\star}}_{\text{variable-property}}. \tag{8.76}$$

Given the collapse of the non-dimensional shear discussed before, it follows that

$$\underbrace{\frac{\mu_t}{\mu_w} = \frac{\mu_t}{\rho_w u_\tau \delta_v} = \mu_t^+}_{\text{constant-property}} \approx \underbrace{\mu_t^\star = \frac{\mu_t}{\bar{\rho} u_\tau^\star \delta_v^\star} = \frac{\mu_t}{\bar{\mu}}}_{\text{variable-property}}. \tag{8.77}$$

This relation is yet another instance that highlights the importance of $u_\tau^\star$ and $\delta_v^\star$ as the characteristic velocity and length scales in the inner layer for variable-property flows, analogous to u_τ and δ_v in constant-property flows. In the following, this equivalence is used to introduce a recipe for developing turbulence model corrections for variable-property flows.

8.4.3 Semi-local scaling framework for turbulence models

In the preceding discussion, we observed that the mean shear and eddy viscosity, when scaled using $u_\tau^\star$ and $\delta_v^\star$ collapses on to their incompressible counterparts as a function of $y^\star = y/\delta_v^\star$. Similarly, various other quantities that are relevant for turbulence modeling, like the turbulent kinetic energy and its dissipation rate, also collapse well when semi-locally scaled (Patel et al., 2016b; Pecnik and Patel, 2017; Zhang et al., 2018). This suggests that $u_\tau^\star$ and $\delta_v^\star$ are the correct characteristic scales in the inner layer of variable-property flows, analogous to u_τ and δ_v in incompressible flows.

On the other hand, in the outer layer of variable-property flows, the inertial effects dominate over the viscous effects, making a viscosity-based length scale $\delta_v^\star$ less relevant. Instead, a characteristic length scale specific to the flow is required, such as δ for a boundary layer or H (half-height) for a channel. Moreover, the outer layer shares the inner-layer velocity scale, $u_\tau^\star$, which is essential to observe a logarithmic velocity profile in the overlap region. In other words, $u_\tau^\star$ and δ are the right characteristic scales in the outer layer of variable-property flows, analogous to u_τ and δ in incompressible flows (Smits and Dussauge, 2006; Hasan et al., 2024). These different scaling approaches are summarized in Table 8.1.

TABLE 8.1 The table presents conventional scaling for constant-property flows alongside semi-local scaling for variable-property flows. In both cases, a distinction is made between inner- and outer-layer scaling. Inner-layer scaling is based on the viscous length scale, denoted as δ_v for constant-property flows and $\delta_v^\star$ for variable-property flows. Outer-layer scaling, on the other hand, is based on a length scale L which corresponds to δ for boundary layers or H (half-height) for channels. Note that the friction velocity scale is shared between the inner- and outer-layer scalings. For constant-property flows, it is represented by u_τ, while for variable-property flows, it becomes $u_\tau^\star$. In the lower rows, several key quantities are provided to highlight their individual scalings.

	Constant properties		**Variable properties**	
	inner-layer $(\cdot)^+$	**outer-layer** $(\cdot)^\oplus$	**inner-layer** $(\cdot)^\star$	**outer-layer** $(\cdot)^\circledast$
Vel. scale	$u_\tau = \sqrt{\tau_w/\rho_w}$		$u_\tau^\star = \sqrt{\tau_w/\bar{\rho}}$	
Len. scale	$\delta_v = \frac{\mu_w}{\rho_w u_\tau}$	L	$\delta_v^\star = \frac{\bar{\mu}}{\bar{\rho} u_\tau^\star}$	L
Wall distance	$y^+ = \frac{y}{\delta_v}$	$y^\oplus = \frac{y}{L}$	$y^\star = \frac{y}{\delta_v^\star}$	$y^\circledast = \frac{y}{L}$
Mean shear	$\frac{d\bar{u}^+}{dy^+} = \frac{\delta_v}{u_\tau}\frac{d\bar{u}}{dy}$	$\frac{d\bar{u}^\oplus}{dy^\oplus} = \frac{L}{u_\tau}\frac{d\bar{u}}{dy}$	$\frac{d\bar{u}^\star}{dy^\star} = \frac{\delta_v^\star}{u_\tau^\star}\frac{d\bar{u}}{dy}$	$\frac{d\bar{u}^\circledast}{dy^\circledast} = \frac{L}{u_\tau^\star}\frac{d\bar{u}}{dy}$
TKE	$k^+ = k^\oplus = \frac{k}{u_\tau^2}$		$k^\star = k^\circledast = \frac{k}{u_\tau^{\star 2}}$	
Turb. diss.	$\varepsilon_V^+ = \frac{\varepsilon_V}{\rho_w u_\tau^3/\delta_v}$	$\varepsilon_V^\oplus = \frac{\varepsilon_V}{\rho_w u_\tau^3/L}$	$\varepsilon_V^\star = \frac{\varepsilon_V}{\bar{\rho} u_\tau^{\star 3}/\delta_v^\star}$	$\varepsilon_V^\circledast = \frac{\varepsilon_V}{\bar{\rho} u_\tau^{\star 3}/L}$
Spec. turb. d.	$\omega^+ = \frac{\omega}{u_\tau/\delta_v}$	$\omega^\oplus = \frac{\omega}{u_\tau/L}$	$\omega^\star = \frac{\omega}{u_\tau^\star/\delta_v^\star}$	$\omega^\circledast = \frac{\omega}{u_\tau^\star/L}$
Eddy visc.	$\mu_t^+ = \frac{\mu_t}{\rho_w u_\tau \delta_v}$	$\mu_t^\oplus = \frac{\mu_t}{\rho_w u_\tau L}$	$\mu_t^\star = \frac{\mu_t}{\bar{\rho} u_\tau^\star \delta_v^\star}$	$\mu_t^\circledast = \frac{\mu_t}{\bar{\rho} u_\tau^\star L}$
Dyn. visc.	$\mu^+ = \frac{\mu_w}{\rho_w u_\tau \delta_v}$	$\mu^\oplus = \frac{\mu_w}{\rho_w u_\tau L}$	$\mu^\star = \frac{\bar{\mu}}{\bar{\rho} u_\tau^\star \delta_v^\star}$	$\mu^\circledast = \frac{\bar{\mu}}{\bar{\rho} u_\tau^\star L}$

At this point we can state the following: If the individual quantities in a variable-property flow, such as μ_t, k or ε, can be scaled by $u_\tau^\star$ and $\delta_v^\star$ (or $u_\tau^\star$ and δ in outer-layer scaling) to collapse their profiles with their constant-property counterparts, then their model equations expressed in the semi-locally scaled form should be analogous to those written in the classically scaled form for a constant-property flow. This idea was proposed by Hasan et al. (2025b), building on the earlier work of Pecnik and Patel (2017) and Otero R. et al. (2018). They then applied this idea to develop a generalized method for deriving variable-property corrections for turbulence models as follows:

1. Write a constant-property turbulence model equation in dimensional form.
2. Scale it using an inner- or outer-scaling framework using the second or the third column in Table 8.1.
3. Replace all the inner $(\cdot)^+$- or outer $(\cdot)^\oplus$-scaled variables in that model equation with the corresponding semi-locally inner $(\cdot)^\star$- or outer $(\cdot)^\circledast$-scaled variables for variable-property flows.
4. Rewrite them in dimensional form using the definitions of the scaled variables in the fourth or the fifth column in Table 8.1.

This implies that a standard off-the-shelf model developed for incompressible, constant-property flows can be applied by substituting its variables with their semi-locally scaled equivalents. The solution of this model will account for mean property variations but will

neglect any correlations with property fluctuations. It is important to note that such a model does not distinguish between a Favre or Reynolds average.

Depending on the scaling framework—inner or outer—different corrections are obtained, resulting in two sets of corrections that may need 'blending' in the overlap region of a boundary layer. The concept of separate scaling laws for the inner and outer layers was first proposed by Hasan et al. (2024) for mixing-length models. Next, this four-step approach just presented is applied to derive variable-property corrections for turbulence models, in particular, for algebraic eddy viscosity expressions in the following section, and for turbulence models based on transport equations in Sect. 8.4.5.

8.4.4 Algebraic eddy-viscosity models

In turbulence modeling, the eddy viscosity is typically determined using dimensional analysis (Pope, 2000), which involves expressing it as the product of a turbulent length and velocity scale, given by

$$\frac{\mu_t}{\rho} \propto \mathcal{U}\mathcal{L}. \tag{8.78}$$

The length scale, $\mathcal{L}$, represents the size of the turbulent eddies, while the velocity scale, $\mathcal{U}$, characterizes the velocity of turbulent fluctuations. Both are determined based on local flow variables. The way these scales are determined commonly classifies the turbulence models into zero (also called algebraic), one, or two equation models.

While algebraic models are not commonly used anymore in RANS modeling, they still hold relevance in wall-modeled large-eddy simulations (Piomelli and Balaras, 2002; Larsson et al., 2016; Bose and Park, 2018; Yang and Lv, 2018; Iyer and Malik, 2019). Considering this, we will mainly discuss the inner-layer algebraic eddy viscosity models that are commonly used in wall-modeling for large-eddy simulations.

Algebraic models are the simplest type of turbulence models since they do not require solving any conservation equations to determine μ_t. Instead, the eddy viscosity is computed in terms of mixing length, analogous to the mean free path in gases. These models are by definition incomplete (Wilcox, 2006) because the mixing length is flow dependent and needs to be specified beforehand using length scales of the mean flow.

8.4.4.1 Prandtl's mixing-length model

Pioneering work in the development of algebraic models was done by Prandtl, who put forth his visualization of turbulent motions in the form of fluid parcels that move in the wall-normal direction and retain their momentum until a distance $\mathcal{L}$, which was termed as the mixing length l_m. Prandtl then reasoned that the velocity scale $\mathcal{U}$ for these parcels can be written, consistent on dimensional grounds, as $l_m|d\bar{u}/dy|$. With these arguments, the eddy viscosity is approximated for constant-property flows as

$$\mu_t = \rho_w \, l_m \, l_m \left|\frac{d\bar{u}}{dy}\right| = \rho_w l_m^2 \left|\frac{d\bar{u}}{dy}\right|. \tag{8.79}$$

Prandtl hypothesized that, for wall-bounded flows, the mixing length is proportional to the distance away from the wall, namely, $l_m = \text{constant} \cdot y$, where the constant is equal to the

von Kármán constant κ. However, close to the wall, the eddy viscosity reduces at a faster rate than κy, attributed to the viscous and inviscid (wall-blocking) damping of turbulent motions close to the wall. To account for this, Van Driest (1956) proposed a damping function such that

$$l_m = \kappa y D(y^+), \tag{8.80}$$

with the damping being a function of wall distance

$$D(y^+) = 1 - \exp\left(\frac{-y^+}{A^+}\right), \tag{8.81}$$

where $A^+ = 26$ was chosen.

With the Van-Driest damping function, the model equation for μ_t is written as

$$\mu_t = \rho_w (\kappa y D(y^+))^2 \left|\frac{d\bar{u}}{dy}\right|. \tag{8.82}$$

We can now apply the four-step approach just described to derive corrections as per the outer- and inner-scaling frameworks.

Outer-layer scaling—Substituting the dimensional quantities in Eq. (8.82) with the outer-scaled ones from Table 8.1, we get

$$\rho_w u_\tau L \, \mu_t^\oplus = \rho_w (\kappa L y^\oplus \, D(y^+))^2 \frac{u_\tau}{L} \left|\frac{d\bar{u}^\oplus}{dy^\oplus}\right|, \tag{8.83}$$

which after simplification gives

$$\mu_t^\oplus = (\kappa y^\oplus \, D(y^+))^2 \left|\frac{d\bar{u}^\oplus}{dy^\oplus}\right|. \tag{8.84}$$

Now, using step 3 from this approach, we replace all the $(\cdot)^\oplus$ variables with their variable-property counterparts as

$$\mu_t^\circledast = (\kappa y^\circledast \, D(y^+))^2 \left|\frac{d\bar{u}^\circledast}{dy^\circledast}\right|, \tag{8.85}$$

where the damping function remains unmodified in the outer-layer scaling framework. As per step 4, we now rewrite the scaled variables in their dimensional form as

$$\frac{\mu_t}{\bar{\rho} u_\tau^\star L} = (\kappa y/L \, D(y^+))^2 \frac{L}{u_\tau^\star} \left|\frac{d\bar{u}}{dy}\right|. \tag{8.86}$$

After simplification, the final form of the eddy viscosity is obtained that is consistent with the outer-layer scaling framework as

$$\mu_t = \bar{\rho} (\kappa y D(y^+))^2 \left|\frac{d\bar{u}}{dy}\right|. \tag{8.87}$$

This formulation is the same as the one for constant-property flows, except that the density at the wall is replaced with the local density.

This correction has in fact been proposed by Van Driest, who replaced ρ_w by $\bar{\rho}$ in Eq. (8.80), while maintaining y^+ in the damping function.

Inner-layer scaling—Eq. (8.82) in the inner-scaled form can be written as

$$\mu_t^+ = (\kappa y^+ D(y^+))^2 \left| \frac{d\bar{u}^+}{dy^+} \right|. \tag{8.88}$$

Using step 3, we replace all the $(\cdot)^+$ variables with their $(\cdot)^*$ counterparts to get

$$\mu_t^\star = (\kappa y^\star D(y^\star))^2 \left| \frac{d\bar{u}^\star}{dy^\star} \right|, \tag{8.89}$$

where, consistent with the inner-layer scaling, we have replaced y^+ with $y^\star$ in the damping function. Rewriting this equation using the dimensional form of the variables, we get, upon simplification,

$$\mu_t = \bar{\rho}(\kappa y D(y^\star))^2 \left| \frac{d\bar{u}}{dy} \right|. \tag{8.90}$$

A comparison of Eqs. (8.87) and (8.90) reveals that the difference between the eddy viscosity derived from the outer- and inner-layer scaling lies solely in the argument of damping function, either y^+ or $y^\star$. The idea of replacing y^+ by $y^\star$ in the damping functions was first proposed by Viala and Aupoix (1995); Catris and Aupoix (2000) for two-equation turbulence models, and more recently by Patel et al. (2016a,b); Yang and Lv (2018); Iyer and Malik (2019) for mixing-length models.

Model results—Throughout this chapter, the focus is on fully developed channel flows that can be modeled as one-dimensional problems. Let us rewrite the stress balance equation in the inner layer of channel flows as

$$\frac{d\bar{u}^\star}{dy^\star} - \frac{\widetilde{\bar{\rho}u''v''}}{\bar{\tau}_w} \approx \frac{\bar{\tau}_t}{\bar{\tau}_w}, \tag{8.91}$$

where $\bar{\tau}_t/\bar{\tau}_w \approx 1 - y/H$. As shown in Bradshaw and Huang (1995), the non-universality in the total shear stress introduced by pressure-gradients in channel flows is balanced by the non-universality in the Reynolds shear stress such that the quantity $-\widetilde{\bar{\rho}u''v''}/\bar{\tau}_w + y/H$ is universal, rather than $-\widetilde{\bar{\rho}u''v''}/\bar{\tau}_w$. Thus, the eddy-viscosity mixing-length models (that are only a function of y^+ or $y^\star$) approximate the quantity $-\widetilde{\bar{\rho}u''v''}/\bar{\tau}_w + y/H$ as $\mu_t^\star(d\bar{u}^\star/dy^\star)$, instead of the Reynolds shear stress alone. This means that, for channel flows, we can write the stress balance equation alternatively as

$$\frac{d\bar{u}^\star}{dy^\star} + \underbrace{\left(-\frac{\widetilde{\bar{\rho}u''v''}}{\bar{\tau}_w} + \frac{y}{H} \right)}_{\mu_t^\star(d\bar{u}^\star/dy^\star)} \approx 1. \tag{8.92}$$

Rewriting this equation in dimensional form, we get

$$\bar{\mu}\frac{d\bar{u}}{dy} + \mu_t\frac{d\bar{u}}{dy} \approx \bar{\tau}_w, \tag{8.93}$$

which is the same as the stress-balance equation for equilibrium boundary layers.

Now, introducing the eddy viscosity from Prandtl's mixing-length model, we get

$$\bar{\mu}\frac{d\bar{u}}{dy} + \bar{\rho}l_m^2\left|\frac{d\bar{u}}{dy}\right|\frac{d\bar{u}}{dy} \approx 1, \tag{8.94}$$

where $l_m = \kappa y D(y^+)$ as per outer-scaling and $l_m = \kappa y D(y^\star)$ as per inner-scaling. Upon simplification, we get a quadratic equation as

$$\bar{\rho}l_m^2\left(\frac{d\bar{u}}{dy}\right)^2 + \bar{\mu}\frac{d\bar{u}}{dy} - \bar{\tau}_w = 0, \tag{8.95}$$

which leads to the solution

$$\frac{d\bar{u}}{dy} = \frac{2\tau_w}{\bar{\mu} + \sqrt{\bar{\mu}^2 + 4\bar{\tau}_w\bar{\rho}l_m^2}}. \tag{8.96}$$

Integrating Eq. (8.96) gives the desired velocity profile.

Fig. 8.5 shows results for the ratio of μ_t/μ (top row) and the semi-locally scaled-velocity profiles $\bar{u}^\star$ (bottom row) using different eddy-viscosity formulations. These individual profiles are computed for three cases and compared to the DNS introduced in Figs. 8.3(a) and (b) (Pecnik and Patel, 2017) and a supersonic channel flow at $M_b = 3$ (Trettel and Larsson, 2016). The results are based on three implementations of eddy viscosity μ_t, namely, for constant properties (Eq. (8.82)), for variable-property with μ_t in its outer-layer- (Eq. (8.87)) and its inner-layer-scaled form (Eq. (8.90)). To solely focus on the results for the momentum equation, the density and viscosity distributions are taken directly from the DNS results. As expected, the constant-property eddy-viscosity formulation performs poorly. The outer-layer-scaled formulation shows some improvement, particularly in capturing the slope of the velocity profile in the logarithmic layer. However, the log-law intercept is too low. The inner-layer-scaled version provides the closest match to the DNS.

8.4.4.2 Johnson–King model

Another common eddy-viscosity model for the inner layer is the one proposed by Johnson and King (1985) and Cabot (1995). It is given as

$$\mu_t = \rho_w u_\tau \kappa y D^2(y^+), \tag{8.97}$$

where the damping function is similar to that proposed by Van Driest for Prandtl's mixing-length model (8.81), except that the constant A^+ is modified to 17.

Following the same approach as that presented for the Prandtl's mixing-length model, we can derive the Johnson–King eddy viscosity as per the outer- and inner-scaling approaches as

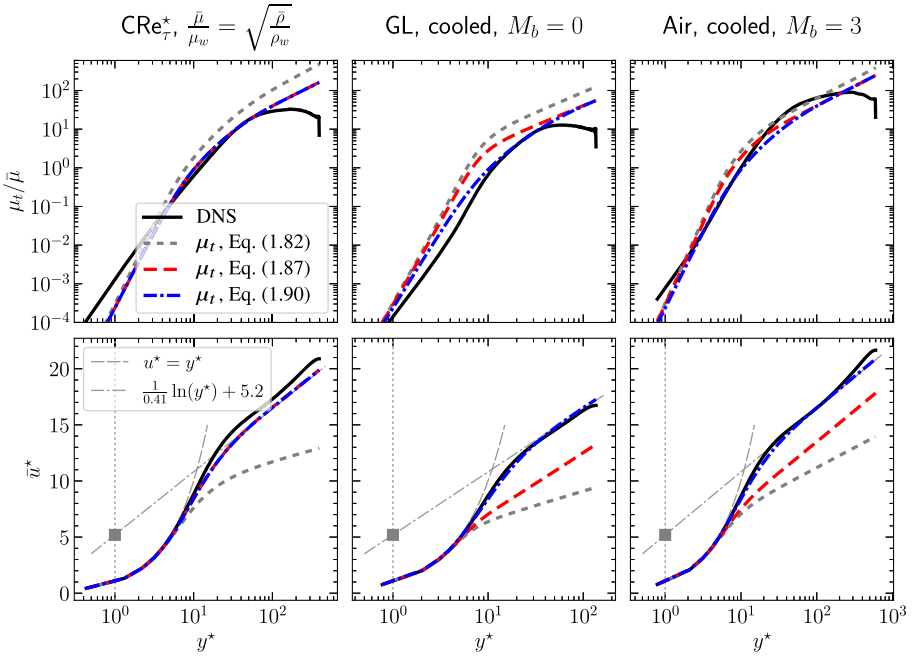

FIGURE 8.5 Eddy viscosity and velocity profiles obtained with three different implementations of the Prandtl mixing-length model. Top row, $\mu_t/\bar{\mu}$, bottom row, $\bar{u}^\star$ as a function of $y^\star$, where $u^\star$ is computed using Eq. (8.72). Columns are: constant semi-local Reynolds number $\mathrm{CRe}^\star_\tau$ and gas-like (GL) cases by Pecnik and Patel (2017), and the supersonic channel flow at bulk Mach number of $M_b = 3$ (where $M_b = u_b/a_w$, with a_w being the sound speed at the wall) by Trettel and Larsson (2016). The dash dotted lines indicate the log-law profile, while the filled gray square indicates the log-law intercept.

Outer-layer scaling—

$$\mu_t = \bar{\rho} u_\tau^* \kappa y D^2(y^+) \tag{8.98}$$

Inner-layer scaling—

$$\mu_t = \bar{\rho} u_\tau^* \kappa y D^2(y^*). \tag{8.99}$$

Like the Prandtl mixing-length model, the difference between the two forms lies only in the damping function. The JK model with the outer-scaled form has been popularly used as an equilibrium wall-model. However, recently, the inner-scaled form of the JK mixing-length model has been shown to improve the results substantially as compared to the outer-layer form (Patel et al., 2016a; Yang and Lv, 2018; Hasan et al., 2024).

8.4.5 Turbulence models based on transport equations

When transport models are used to model the eddy viscosity, the velocity scale in Eq. (8.78) is usually based on the square-root of the turbulent kinetic energy k, and the turbulent length

scale can be estimated using k and the turbulent dissipation rate ε or the specific turbulent dissipation rate $\omega \propto \varepsilon/k$, among others. For example,

$$\frac{\mu_t}{\rho} \propto \sqrt{k} l_t \propto \frac{k^2}{\varepsilon_M} \propto \frac{k}{\omega}, \tag{8.100}$$

where l_t is a turbulent length scale, ε_M is the turbulent dissipation rate per unit mass, and ω the specific turbulent dissipation rate. Many more possible relations for the eddy viscosity can be found in the literature. The reader is referred to Pope (2000).

The turbulence models that provide these scales (such as $k-\varepsilon$ and $k-\omega$) were originally developed and calibrated for incompressible flows. The model constants were tuned for canonical cases, where the transport equations can be simplified, allowing individual constants to be determined for those specific cases.

However, the challenge arises when adapting these models for compressible flows, specifically for effects related to heat transfer (variable mean properties) and intrinsic compressibility at high Mach numbers. Early attempts at introducing compressibility corrections for boundary layers were inspired by turbulence modeling of free shear layers. These corrections primarily focused on adapting the models for intrinsic compressibility effects, such as pressure dilatation and dilatational dissipation, to the turbulent kinetic energy equation. For example, Zeman (1990) proposed a dilatational dissipation model for high-speed free-shear flows, which was later extended to wall-bounded flows by Zeman (1993).

Although these models were applied to wall-bounded flows with some success, improvements were often for reasons unrelated to intrinsic compressibility effects (Rumsey, 2010). In fact, as shown by Huang et al. (1995), these compressibility effects are negligible in wall-bounded flows for bulk Mach numbers up to 3.

Another approach in sensitizing turbulence models for compressibility effects dates back to Huang et al. (1994). For instance, Huang et al. (1994) analytically showed that the turbulence model constants must be functions of the mean density gradient in order to achieve the correct log-layer slope of the Van Driest transformed velocity profile of a modeled high-speed boundary layer. Although insightful, this approach appeared impractical as it requires modifications of the standard-model constants.

8.4.5.1 Compressibility correction by Catris and Aupoix

Later, Catris and Aupoix (2000) argued that the density dependence from the model constants can be eliminated by modifying the model for the turbulent diffusion in the turbulence model equations. The turbulent diffusion is commonly modeled with the gradient diffusion hypothesis, see Eq. (8.39). With it, the TKE equation (8.51) can be written for the log-layer region, where advection, viscous diffusion, and compressibility effects are small, as

$$P - \bar{\rho}\varepsilon_M + \frac{d}{dy}\left(\frac{\mu_t}{\sigma_k}\frac{dk}{dy}\right) \approx 0. \tag{8.101}$$

Since in the log-layer, production and dissipation must be balanced (Smits and Dussauge, 2006), the turbulent diffusion must be zero. However, in a boundary layer where density is varying, the turbulent diffusion as given here will not vanish. The reason is as follows.

In an equilibrium constant stress zone, the turbulent shear stress is $-\widetilde{\bar{\rho}u''v''} \approx \rho_w u_\tau^2$. Since $k \propto \widetilde{u''v''}$, also $\bar{\rho}k$ must be constant. However, a variation in $\bar{\rho}$ in the log-layer of a compressible boundary layer will necessarily result in a corresponding variation of k. As such, the model for the turbulent diffusion is non-zero and the balance between production and dissipation in the log-law region is altered. This modeling issue has, in fact, been known since Shih et al. (1987).

Catris and Aupoix (2000) proposed a remedy to this. They argued that the turbulent diffusion of TKE acts upon the energy per unit volume (Joule/m^3) of turbulent fluctuations, which is ρk. Therefore, the turbulent diffusion of TKE is based on $\bar{\rho}k$, while the diffusion coefficient is divided by the density based on dimensional consistency. Their formulation of the turbulent diffusion term of TKE is then

$$P - \bar{\rho}\varepsilon_M + \frac{d}{dy}\left[\frac{1}{\bar{\rho}}\frac{\mu_t}{\sigma_k}\frac{d\,(\bar{\rho}k)}{dy}\right] \approx 0. \tag{8.102}$$

This model for the turbulent diffusion vanishes in the log-layer, and the balance between production and dissipation is respected. They also formulated corresponding diffusion-term modifications for the transport equations of the turbulent length scale and the (specific) turbulent dissipation rate.

This approach, by design, only accounts for variable density in the log-layer to recover the correct slope of the Van Driest scaled-velocity profile. In other words, it only accounts for changes in friction velocity scale (see also Eq. (8.66)). However, we know that, in the inner layer, changes in viscous length scales must be accounted for, as also evident from the velocity transformation (see Eq. (8.72)).

In the following, we will first outline how an analogous correction to Catris and Aupoix (2000) can be derived using the semi-local scaling framework described in Sect. 8.4.3. Following this, a discussion is given on how the semi-local scaling framework can also be used to derive turbulence-model corrections that are consistent with inner-layer scaling, accounting for variations in both the viscous length and friction velocity scales.

8.4.5.2 Application of the semi-local scaling framework

The approach outlined in Sect. 8.4.3 will now be applied to derive corrections for transport equations of turbulence models, ensuring consistency with the semi-local scaling framework (Hasan et al., 2025b), similar to the discussion of the algebraic turbulence model discussed in the previous section. These corrections can be derived in two ways: using either inner-layer or outer-layer scaling. By applying outer-layer scaling, the correction proposed by Pecnik and Patel (2017) and Otero R. et al. (2018), which is similar to the one introduced by Catris and Aupoix (2000), can be obtained. This will be discussed next.

Outer-layer scaling—We begin by stating the dimensional form of the TKE equation for an incompressible, constant-property fully developed turbulent channel flow. In this case, the TKE equation (8.51) reduces to a balance equation between production, dissipation and diffusion of TKE as

$$\mu_t\left(\frac{d\bar{u}}{dy}\right)^2 - \varepsilon_V + \frac{d}{dy}\left[\left(\mu_w + \frac{\mu_t}{\sigma_k}\right)\frac{dk}{dy}\right] = 0. \tag{8.103}$$

Next, applying the constant-property, outer-layer scaling (see third column in Table 8.1) and then dividing the entire equation by $\rho_w u_\tau^3/L$, we obtain the non-dimensional form as

$$\mu_t^{\oplus}\left(\frac{d\bar{u}^{\oplus}}{dy^{\oplus}}\right)^2-\varepsilon_V^{\oplus}+\frac{d}{dy^{\oplus}}\left[\left(\mu^{\oplus}+\frac{\mu_t^{\oplus}}{\sigma_k}\right)\frac{dk^{\oplus}}{dy^{\oplus}}\right]=0. \tag{8.104}$$

We now enforce the strict analogy between constant- and variable-property flows by replacing the classically scaled variables by their semi-locally scaled equivalents (replacing $\oplus$ with $\circledast$; step 3 in Sect. 8.4.3). This gives

$$\mu_t^{\circledast}\left(\frac{d\bar{u}^{\circledast}}{dy^{\circledast}}\right)^2-\varepsilon_V^{\circledast}+\frac{d}{dy^{\circledast}}\left[\left(\mu^{\circledast}+\frac{\mu_t^{\circledast}}{\sigma_k}\right)\frac{dk^{\circledast}}{dy^{\circledast}}\right]=0. \tag{8.105}$$

To return to the dimensional form, we substitute the expressions from the fifth column in Table 8.1, to get

$$\frac{\mu_t}{\bar{\rho}u_\tau^\star L}\left(\frac{L}{u_\tau^\star}\right)^2\left(\frac{d\bar{u}}{dy}\right)^2-\frac{L}{\bar{\rho}u_\tau^{\star 3}}\varepsilon_V+\frac{d}{d\,(y/L)}\left[\frac{1}{\bar{\rho}u_\tau^\star L}\left(\bar{\mu}+\frac{\mu_t}{\sigma_k}\right)\frac{d(k/u_\tau^{\star 2})}{d\,(y/L)}\right]=0. \tag{8.106}$$

Simplifying this equation and using the definition of the semi-local friction velocity, $u_\tau^\star$, we finally get

$$\mu_t\left(\frac{d\bar{u}}{dy}\right)^2-\varepsilon_V+\frac{1}{\sqrt{\bar{\rho}}}\frac{d}{dy}\left[\frac{1}{\sqrt{\bar{\rho}}}\left(\bar{\mu}+\frac{\mu_t}{\sigma_k}\right)\frac{d(\bar{\rho}k)}{dy}\right]=0. \tag{8.107}$$

This form is the same as that proposed in Otero R. et al. (2018).

Interestingly, this form is also very similar to the one proposed by Catris and Aupoix (2000) as the diffusion is also a function of $\bar{\rho}k$. However, compared to the correction proposed by Catris and Aupoix (2000), two key differences can be seen. The first difference concerns the treatment of the viscous diffusion of the TKE. In Eq. (8.102), the viscous diffusion of TKE remains unchanged, which is consistent with the derivation presented earlier in Eq. (8.38). In contrast, the semi-local scaling approach modifies not only the turbulent but also viscous diffusion as a function of $\bar{\rho}k$. This modification arises from the assumption that the entire diffusion of TKE is taken as part of the turbulence model to which the semi-local scaling is applied. The second difference lies in the diffusion coefficient. Based on dimensional consistency, Catris and Aupoix (2000) proposed a coefficient of $1/\bar{\rho}$, while Otero R. et al. (2018) derived the diffusion coefficient and the factor of the whole diffusion term to be $1/\sqrt{\bar{\rho}}$.

Repeating the same steps for the dissipation rate equation, a generic version of a $k-\varepsilon$ turbulence model is

$$\begin{aligned}
\bar{\rho}\frac{Dk}{Dt}&=P-\bar{\rho}\varepsilon_M+\frac{1}{\sqrt{\bar{\rho}}}\frac{\partial}{\partial x_i}\left[\frac{1}{\sqrt{\bar{\rho}}}\left(\bar{\mu}+\frac{\mu_t}{\sigma_k}\right)\frac{\partial\,(\bar{\rho}k)}{\partial x_i}\right],\\
\bar{\rho}\frac{D\varepsilon_M}{Dt}&=\frac{1}{T}\left(C_{\varepsilon 1}P-C_{\varepsilon 2}\bar{\rho}\varepsilon_M\right)+\frac{1}{\bar{\rho}}\frac{\partial}{\partial x_i}\left[\frac{1}{\sqrt{\bar{\rho}}}\left(\bar{\mu}+\frac{\mu_t}{\sigma_\varepsilon}\right)\frac{\partial\left(\bar{\rho}^{3/2}\varepsilon_M\right)}{\partial x_i}\right],
\end{aligned} \tag{8.108}$$

where the diffusion-term corrections for the ε_M equation are the same as those proposed in Otero R. et al. (2018) and Catris and Aupoix (2000). The turbulence production P is modeled as given in Eq. (8.52), and the turbulence time scale is defined as $T = k/\varepsilon_M$. The model parameters, as well as any near-wall damping functions, for a specific version of the $k-\varepsilon$ turbulence model remain unaltered, except that y^+ in these damping functions is replaced by $y^\star$ as proposed by Viala and Aupoix (1995); Catris and Aupoix (2000); Otero R. et al. (2018) to account for changes in viscous length scales. This modification of the wall-normal coordinate in the damping function is consistent with the inner-layer-scaling framework, which as discussed later, plays an important role in improving the accuracy of the results.

Model results, outer-layer scaling—To demonstrate how well these variable-property corrections work for both low Mach number and high Mach-number channel flows, we will apply the $k-\varepsilon-\overline{v'^2}-f$ (V2F) turbulence model (Durbin, 1995) for the same cases as shown in Fig. 8.5. The V2F model is chosen because it provides accurate solutions of turbulence kinetic energy k and dissipation rate ε, unlike conventional $k-\varepsilon$ models. Conventional $k-\varepsilon$ models use damping functions or additional source terms that negatively affect the accuracy of k and ε distributions at the cost of providing accurate solutions of the eddy viscosity. The V2F model, instead, includes a transport equation for the wall-normal velocity fluctuation $\overline{v'^2}$, which is the proper velocity scale for turbulent transport towards the wall, and an elliptic relaxation equation that incorporates the correct near-wall damping of the eddy viscosity without compromising the accuracy of k and ε. This allows for a more rigorous assessment of the effectiveness of the compressibility corrections when comparing these turbulence quantities obtained from the model with those from DNS. For the compressibility corrections, the diffusion terms in the k, the ε and the $\overline{v'^2}$ equations are changed accordingly, while the f equation remains unchanged (Pecnik and Patel, 2017).

The results are shown in Fig. 8.6. The columns show the same three cases as presented in Fig. 8.5. The rows depict the semi-locally scaled-velocity profile, the turbulent shear stress, the turbulent kinetic energy, and the turbulent dissipation rate. Clearly, when compared to the standard turbulence-model formulation, the models incorporating the modified diffusion significantly improve the results. This improvement is especially noticeable in the k profiles (third row). Interestingly, for k, the approach by Otero R. et al. (2018) yields slightly more accurate results than the method proposed by Catris and Aupoix (2000).

We can also compare the dissipation from the turbulence models with that available from the DNS. Note that the dissipation from the DNS is computed as described in Pecnik and Patel (2017), where it is calculated using semi-locally scaled-velocity fluctuations. The DNS dissipation is presented only for the $\mathrm{CRe}_\tau^\star$ case for which the viscous length scale is constant. For the other cases a comparison with DNS is not shown because, as we will discuss later, accounting for changes in viscous length scale would be necessary in the model equations. When comparing the DNS dissipation for the $\mathrm{CRe}_\tau^\star$ case, we see that the model, as proposed by Otero R. et al. (2018), provides very accurate results. This is an important observation, and it can be explained as follows. Close to the wall the turbulent dissipation rate is balanced by the viscous diffusion of turbulent kinetic energy. Hence, an accurate prediction of near-wall dissipation is connected to an accurate model of the viscous diffusion term of turbulent kinetic energy. This implies that the viscous diffusion should be computed using $(1/\sqrt{\bar{\rho}})d/dy[(\bar{\mu}/\sqrt{\bar{\rho}})d(\bar{\rho}k)/dy]$ rather than $d/dy(\bar{\mu}dk/dy)$ as in Catris and Aupoix (2000).

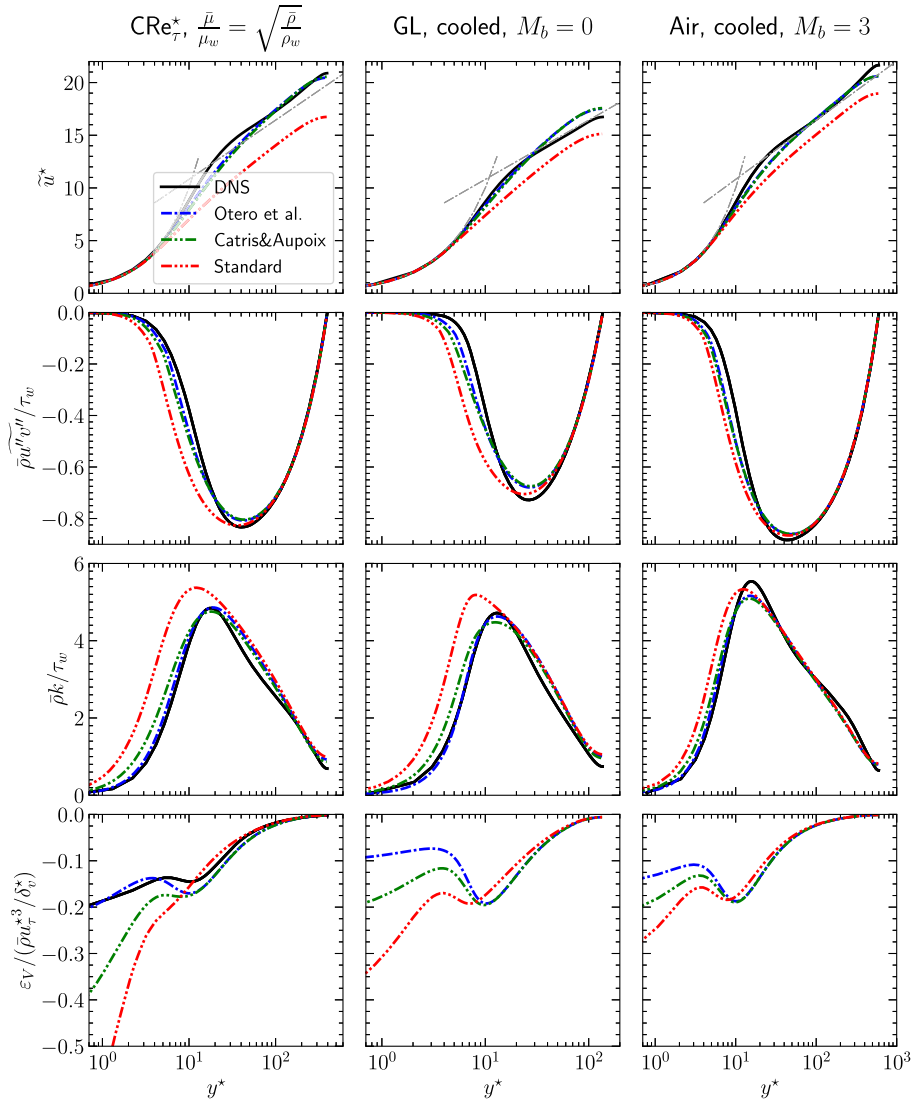

FIGURE 8.6 V2F turbulence modeling results compared to DNS for the constant semi-local Reynolds number $\mathrm{CRe}^\star_\tau$ and gas-like (GL) cases by Pecnik and Patel (2017), and the supersonic channel flow at bulk Mach number of $M_b = 3$ by Trettel and Larsson (2016) (the same cases as presented in Fig. 8.5). The rows correspond to the semi-local velocity transformation, the turbulent shear stress, the turbulent kinetic energy, and the dissipation rate. The modeled dissipation rate $\hat\varepsilon_M$ is compared to the $\hat\varepsilon_V$ from DNS for consistency.

The performance of changing the diffusion term according to the semi-local scaling has also been tested for other turbulence models, such as the models by Spalart and Allmaras (1992); Menter (1994); Myong and Kasagi (1990) in the work by Otero R. et al. (2018), and Smith (1995); Chien (1982) in the work of Catris and Aupoix (2000). Results with the Spalart

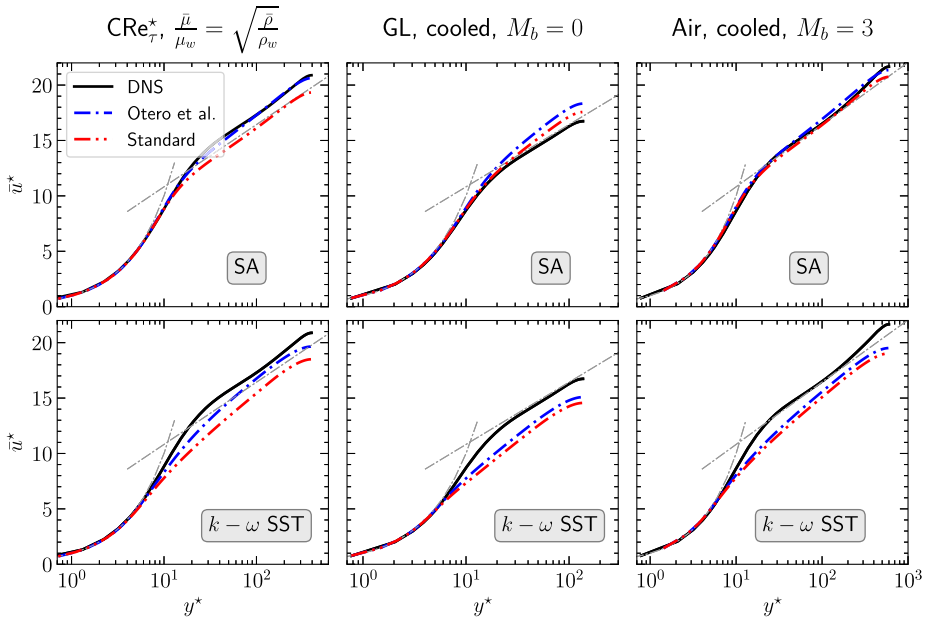

FIGURE 8.7 Results for the Spalart & Allmaras (SA) and Menter's $k-\omega$ SST models for the same cases as presented in Fig. 8.6.

and Allmaras (SA) and Menter's $k-\omega$ (SST) model are shown in Fig. 8.7. Interestingly, the SA model accurately reproduces the velocity profiles for all cases without applying any modifications. A further improvement, using the variable property modifications, can only be achieved for the C$Re^\star_\tau$ case. On the other hand, the SST model does not provide much better results when compared with the DNS. The apparent log-law intercept is too low.

The reason for this is that these corrections are strictly valid only in the outer layer, since the semi-local scaling with the length scale L has been used (Hasan et al., 2025b). As such, they do not account for variations in viscous length scale $\delta^\star_v$ in the inner layer. Despite this limitation, the results for the velocity profile are still accurate for the V2F, the SA and other conventional $k-\varepsilon$ models (not shown). This is because the variations in the viscous length scale are taken into account in a different manner. For instance, Hasan et al. (2025b) summarizes that changes in viscous length scale are accounted for in the:

- k-ε models: using $y^\star$ instead of y^+ in the damping functions;
- Spalart–Allmaras model: through the damping function f_{v1} that uses a semi-locally consistent parameter $\chi = \nu^{\mathrm{SA}}/\bar{\nu} = \nu^{\mathrm{SA}}/(u^\star_\tau \delta^\star_v)$;
- V2F model: with the length scale L_t that switches from $k^{1.5}/\varepsilon$ to the Kolmogorov length scale η in the vicinity of the wall which is proportional to $\delta^\star_v$ (Patel et al., 2016b).

However, accounting for changes in viscous length scales due to property variations as just described is not robust and fails for turbulence models without damping functions, as shown for the k-ω SST model (Menter, 1994). Thus, the inner-layer semi-local scaling approach must be adopted.

Inner-layer scaling—For the inner layer scaling one has to repeat the scaling procedure as described before, but instead use the definitions of the semi-locally scaled quantities for the inner layer (columns two and four of Table 8.1). After applying the constant-property, inner-layer scaling and then replacing all $(\cdot)^+$ with $(\cdot)^\star$, we obtain

$$\mu_t^\star \left(\frac{d\bar{u}^\star}{dy^\star}\right)^2 - \varepsilon_V^\star + \frac{d}{dy^\star}\left[\left(\mu^\star + \frac{\mu_t^\star}{\sigma_k}\right)\frac{dk^\star}{dy^\star}\right] = 0. \tag{8.109}$$

Substituting the $(\cdot)^\star$ quantities with their expressions in column four of Table 8.1, we get

$$\frac{\mu_t}{\bar{\rho}u_\tau^\star \delta_v^\star}\left(\frac{\delta_v^\star}{u_\tau^\star}\right)^2\left(\frac{d\bar{u}}{dy}\right)^2 - \frac{\delta_v^\star}{\bar{\rho}u_\tau^{\star 3}}\varepsilon_V + \frac{d}{d\left(y/\delta_v^\star\right)}\left[\left(1 + \frac{1}{\sigma_k}\frac{\mu_t}{\bar{\rho}u_\tau^\star \delta_v^\star}\right)\frac{d(k/u_\tau^{\star 2})}{d\left(y/\delta_v^\star\right)}\right] = 0, \tag{8.110}$$

which, with the definitions of $\delta_v^\star$ and $u_\tau^\star$ and subsequent simplifications, gives

$$\mu_t\left(\frac{d\bar{u}}{dy}\right)^2 - \varepsilon_V + \frac{1}{\bar{\mu}}\frac{d}{d(y\sqrt{\bar{\rho}}/\bar{\mu})}\left[\left(\mu + \frac{\mu_t}{\sigma_k}\right)\frac{1}{\bar{\mu}}\frac{d(\bar{\rho}k)}{d(y\sqrt{\bar{\rho}}/\bar{\mu})}\right] = 0. \tag{8.111}$$

Compared to the outer-layer scaled TKE in Eq. (8.107), the argument of the diffusion term, $\bar{\rho}k$, remains unchanged. However, the derivatives in the wall-normal direction are evaluated along a modified coordinate that is either stretched or compressed as a function of $\sqrt{\bar{\rho}}/\bar{\mu}$. This effectively accounts for variations in viscous length scales along this direction. To facilitate the implementation of this modification in existing CFD solvers, Hasan et al. (2025b) reformulated this modification such that the conventional diffusion can be used, while the modification is added as an additional source term. Additionally, they proposed a method for blending the inner-layer- and the outer-layer-scaling approaches. This same formulation has also been applied to obtain the ω equation.

The results are shown in Fig. 8.8. Clearly, the results with the inner-layer-scaling approach are improved for the GL and the $M_b = 3$ cases. As expected, for the $\mathrm{CRe}_\tau^\star$ case, where $\sqrt{\bar{\rho}/\bar{\rho}_w} = \bar{\mu}/\bar{\mu}_w$, both scaling approaches give the same results since the viscous length scale (proportional to the inverse of the semi-local Reynolds number) is constant.

8.4.5.3 Applicability limits of the semi-local scaling framework

The validity of the semi-local scaling approach can be best expressed as follows. Starting from the semi-locally scaled continuity and momentum equations, Pecnik and Patel (2017) derived a semi-local turbulent kinetic energy (TKE) equation based on the outer-layer-scaling approach. This TKE equation is essentially equivalent to the incompressible TKE equation, except for the appearance of some additional terms. These terms depend on the normalized density gradient, expressed as

$$d_i = \left(\frac{L}{2\bar{\rho}}\frac{\partial\bar{\rho}}{\partial x_i}\right). \tag{8.112}$$

For the cases they investigated, the terms dependent on d_i were small. However, in cases with very strong density gradients, d_i, and hence the terms dependent on it may no longer be negligible, leading to the semi-local scaling framework being less effective.

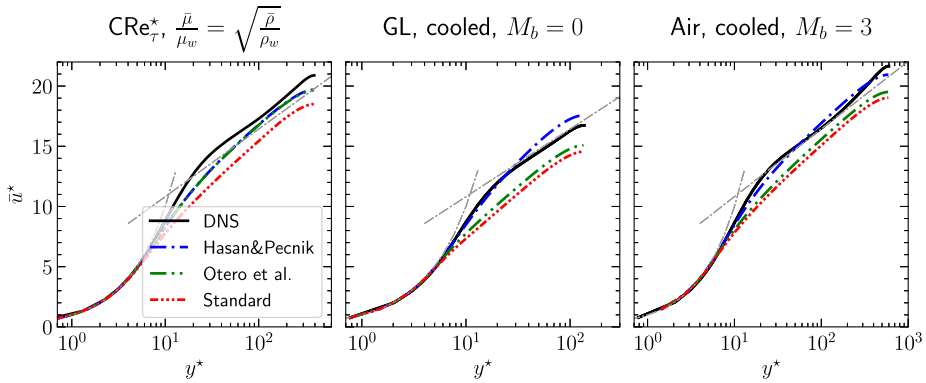

FIGURE 8.8 Results for Menter's $k-\omega$ SST models for the same cases as presented in Fig. 8.6. The inner-layer- and outer-layer-scaling approaches are compared to the standard unmodified model and the DNS results.

Interestingly, d_i is connected to an implicit assumption of Morkovin's hypothesis, namely, that density only changes marginally across an eddy (Bradshaw, 1977). This relationship can be expressed as follows. For wall-bounded flows, where the dominant variation of density occurs in the wall-normal direction, the fractional change of density across an eddy could be estimated as

$$\frac{\Delta\rho}{\bar{\rho}} \approx \frac{1}{\bar{\rho}}\frac{d\bar{\rho}}{dy} L_{eddy}, \tag{8.113}$$

where L_{eddy} measures the eddy size in the wall-normal direction. Comparing Eqs. (8.112) and (8.113), it becomes clear that d_2 (i.e., d_i in the wall-normal direction) signifies the fractional density change across eddies whose length scales are of the order of the outer-layer length scale L.

Eq. (8.113) can also be expressed as a ratio of the eddy length scale and a density-based length scale as

$$\frac{\Delta\rho}{\bar{\rho}} \approx \frac{L_{eddy}}{L_{\rho,2}}, \tag{8.114}$$

where

$$L_{\rho,2} = \left(\frac{1}{\bar{\rho}}\frac{d\bar{\rho}}{dy}\right)^{-1} \tag{8.115}$$

signifies the distance over which density change is of the order of $\bar{\rho}$.

We can now summarize the discussion in this section in terms of different length scales. For cases where the density-based length scale $L_{\rho,2}$ is much larger than the eddy length scale L_{eddy}, Morkovin's assumption of local scaling holds, and, for these cases, we would also expect d_2 to be small, thereby affirming the validity of semi-local scaling as per Pecnik and Patel (2017).

8.5 Modeling intrinsic compressibility effects

At higher Mach numbers, intrinsic compressibility effects become important. In the past, models associated with direct intrinsic compressibility terms, such as pressure dilatation and dilatational dissipation, were proposed for wall-bounded flows, inspired by their respective models for shear layers. Rumsey (2010) observed that using the dilatational dissipation model of Zeman (1993) in the turbulent kinetic energy equation provides just the right amount of reduction in the eddy viscosity to improve skin friction predictions for cooled-wall turbulent boundary layers. However, these models are suspected to not capture the correct physics since in reality both dilatational dissipation and pressure dilatation are negligible in wall-bounded flows (Huang et al., 1995; Zhang et al., 2018). In fact, Zeman (1993) raised the question: "*are (intrinsic) compressibility effects significant in reality, and can they be isolated in experiments and verified?*".

8.5.1 Constant-property compressible turbulent channel flows

The question posed by Zeman (1993) was addressed by Coleman et al. (1995) and more recently by Hasan et al. (2023) and Hasan et al. (2025a). They isolated intrinsic compressibility effects in numerical simulations by conducting DNS at high Mach numbers, $M_b > 1$, but without the appearance of mean property variations. To achieve this, Coleman et al. (1995) suggested to eliminate the viscous heating term ($\tau_{ij}\partial u_i/\partial x_j$) from the internal energy equation. This term drives temperature gradients and, consequently, property variations in high-speed flows. By removing it, the simulations maintain nearly uniform mean temperature, density, and viscosity, enabling a detailed study of intrinsic compressibility effects.

Following this approach, Hasan et al. (2023) formulated four constant-property (CP) cases with bulk Mach numbers of 0.3, 2.28, 3, and 4, and a friction Reynolds number of 550. Fig. 8.9(a) shows the mean velocity profiles for these cases. The case at Mach 0.3 follows the law of the wall, and collapses with the incompressible case of Moser et al. (1999) at a similar Reynolds number. With an increase in Mach number, a clear shift in the log-law profile is observed. Fig. 8.9(b) shows the corresponding turbulent shear stress profiles. An apparent outward shift in the buffer layer is observed with increasing Mach number. The upward shift in the logarithmic velocity profile is directly related to an outward shift in the Reynolds shear stress. This is because an outward shift in the turbulent shear stress implies an outward shift in the viscous shear stress (such that the total shear stress remains unaffected). Since the law of the wall is an integration of the viscous shear stress, its outward shift is responsible for the upward shift in the log-law. In a follow-up study, Hasan et al. (2025a) explained the mechanism through which intrinsic compressibility effects modulate the near-wall dynamics of turbulence, thereby explaining the observed shifts in the velocity and shear stress profiles.

A similar upward shift is also observed in the logarithmic portion of the semi-locally transformed mean-velocity profiles for conventional high Mach-number boundary layers (Trettel and Larsson, 2016; Patel et al., 2016b; Zhang et al., 2018; Griffin et al., 2021). In order to comment whether this shift is due to intrinsic compressibility effects, it is first important to quantify these effects.

To quantify intrinsic compressibility effects, a suitable parameter is needed. Turbulence models in their current form mainly use the turbulence Mach number $M_t = \sqrt{2k}/\bar{a}$ (where $\bar{a}$

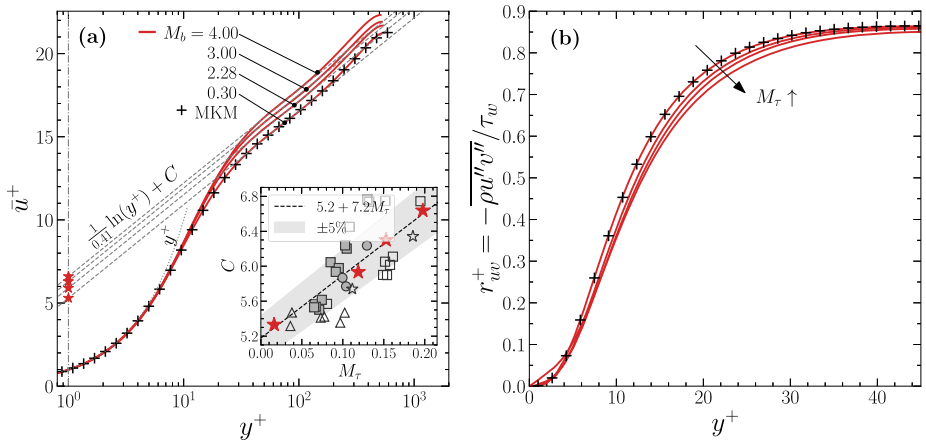

FIGURE 8.9 (a) Mean velocity and (b) Reynolds shear stress profiles for the four CP cases. Black symbols denote the incompressible case of Moser et al. (1999) at $Re_\tau \approx 590$. (adapted from Hasan et al. (2023)).

is the local sound speed) as a measure of intrinsic compressibility effects (for e.g., Sarkar et al., 1991; Wilcox, 1992; Zeman, 1993). However, for boundary layers, Bradshaw (1977) and Smits and Dussauge (2006) suggested the friction Mach number $M_\tau = u_\tau/a_w$ to be a more suitable parameter. Using pressure scaling arguments, Hasan et al. (2023) provided further support for M_τ being the correct parameter for wall-bounded flows. These arguments are substantiated by the observations in Yu et al. (2022), where the friction Mach number was found to adequately quantify intrinsic compressibility effects on wall-pressure and wall-shear-stress fluctuations.

In the semi-local scaling framework, using local properties, the semi-local friction Mach number can be defined as $M_\tau^\star = u_\tau^\star/\bar{a}$. For ideal-gas flows, $u_\tau^\star \sim \sqrt{\bar{T}}$, and thus $M_\tau^\star = u_\tau^\star/\sqrt{\gamma R\bar{T}}$ is roughly constant and equal to M_τ at the wall (Hasan et al., 2025a). This locally constant nature of the friction Mach number makes it a very suitable choice to quantify intrinsic effects when compared to other parameters that vary in the domain (for e.g. M_t).

Taking M_τ as the most appropriate parameter, Hasan et al. (2023) quantified the log-law intercept for the four constant-property cases and for several conventional channels and boundary layers, as shown in the inset of Fig. 8.9(a). As seen from the inset, the conventional cases (gray symbols) follow the trend set by constant-property cases (red stars), signifying that the log-law shift in those cases is also due to intrinsic compressibility effects.

Since the intrinsic compressibility effects are not limited to these four tailored cases, but are also present in conventional cases, it is important to account for these effects in turbulence models. A discussion will follow on the intrinsic compressibility corrections in zero- and two-equation eddy-viscosity-based turbulence models.

8.5.2 Algebraic eddy viscosity models

The intrinsic compressibility effects on turbulent shear stress are confined to the inner layer, as shown in Fig. 8.9(b). Therefore, the following discussion will focus solely on algebraic eddy-viscosity models consistent with the inner-scaling framework.

8.5.2.1 *Johnson–King model*

The Johnson–King model for variable-property flows is given as (restating Eq. (8.99))

$$\mu_t = \bar{\rho} u_\tau^\star \kappa y D^2(y^\star). \tag{8.116}$$

Solving the momentum equation with this eddy viscosity results in a perfect collapse of the semi-locally scaled-velocity profile with the incompressible, constant-property law of the wall. However, as seen in Fig. 8.9(a), with increasing M_τ the velocity profiles show an increase in the log-law intercept. This upward shift can be traced back to an outward shift in the turbulent shear stress profile, as just outlined. Thus, to account for the outward shift in the shear stress profile, and hence an upward shift in the mean velocity profile, Hasan et al. (2023) proposed to increase the damping constant in the eddy-viscosity formulation (8.116) as a function of M_τ. They proposed

$$D(y^\star, M_\tau) = 1 - \exp\left(\frac{-y^\star}{A^+ + f(M_\tau)}\right), \tag{8.117}$$

where the additional function $f(M_\tau)$ was tuned to be equal to $19.3M_\tau$. The increase in the effective damping constant $A^+ + 19.3M_\tau$, where $A^+ = 17$ for $\kappa = 0.41$, implies that the eddy viscosity (and hence, turbulent shear stress) shifts outwards, replicating the desired behavior.

Eq. (8.116), along with the modified damping function (8.117), can be directly applied as a wall model for large eddy simulations. Furthermore, this eddy viscosity correction can serve as a foundation for enhancing other RANS models. For example, the damping function in the mixing lengths of the Cebeci–Smith (Smith and Cebeci, 1967) and Baldwin–Lomax (Baldwin and Lomax, 1978) algebraic models can be modified accordingly. Additionally, as highlighted in Sect. 8.5.3.3, these corrections lead to adjustments in two-equation models.

Model results—The corrected Johnson–King (JK) model, as presented in Eqs. (8.116) and (8.117), is applied for the high Mach-number constant-property channel flows. The mean velocity profile is obtained by integrating the stress balance equation as

$$\bar{u} = \int_0^y \frac{\tau_w}{\bar{\mu} + \mu_t} dy. \tag{8.118}$$

Fig. 8.10 shows the velocity profile for the Mach 2.28, Mach 3, and Mach 4 CP cases. Clearly, the intrinsic-compressibility-corrected JK model reproduces the DNS velocity profile, whereas the JK model without this correction is inaccurate.

Recently, Hasan et al. (2024) tested the modified JK model in combination with an outer-layer-scaled Coles wake function and observed that the corrections reproduce DNS velocity profiles accurately for a wide range of high-speed turbulent boundary layers. To replicate their results, refer to the Jupyter-Notebook (Pecnik and Hasan, 2023).

8.5.2.2 *Prandtl's mixing-length model*

To enhance the Prandtl's mixing length models to account for intrinsic compressibility effects, the damping function needs to be modified as in Eq. (8.117), except that $f(M_\tau) = 39M_\tau$ (Hasan et al., 2024) with $\kappa = 0.41$ and $A^+ = 26$.

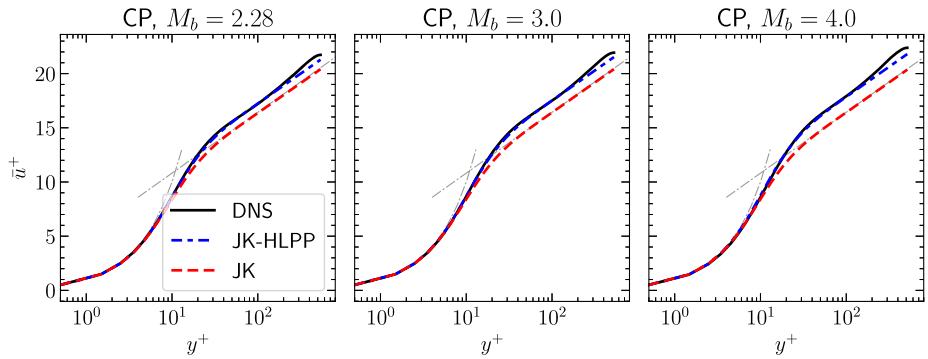

FIGURE 8.10 Mean-velocity profile computed using the Johnson–King (JK) model with and without the compressibility correction of Hasan et al. (2023), Eq. (8.117).

8.5.3 Turbulence models based on transport equations

The state-of-the-art in modeling intrinsic compressibility effects for two-equation models mainly involves the direct compressibility terms in the turbulent kinetic energy equation. These are the dilatational dissipation $\varepsilon_{M,d}$ (per unit mass) and the pressure dilatation terms Π_d.

In the past, significant effort has been devoted to developing $\varepsilon_{M,d}$ and Π_d models for shear layers. These models are then extended with or without any modifications for wall-bounded flows. In the following, we will briefly mention some of these dilatational dissipation and pressure dilatation models and present their results for the four CP cases just discussed.

8.5.3.1 Sarkar–Zeman–Wilcox dilatation–dissipation correction

Zeman (1990), Sarkar et al. (1991) and Wilcox (1992) modeled the dilatation dissipation rate to be proportional to the solenoidal dissipation rate (per unit mass), namely,

$$\varepsilon_{M,d} = \xi^* F(M_t) \varepsilon_{M,s}, \tag{8.119}$$

where $\varepsilon_{M,s}$ is the solenoidal dissipation, ξ^* is a closure coefficient, and $F(M_t)$ is a Mach-number-dependent function. For compressible mixing layers, Zeman (1990) proposed

$$F(M_t) = \left[1 - e^{-(M_t - M_{t_o})^2/\Lambda^2}\right] \mathcal{H}(M_t - M_{t_o}) \quad \text{and} \quad \xi^* = 0.75, \tag{8.120}$$

where $M_{t_0} = 0.1$ and $\Lambda = 0.6$, and $\mathcal{H}(x)$ is a Heaviside step function. For boundary layers, Zeman (1993) further modified the constants to $M_{t_0} = 0.2$ and $\Lambda = 0.66$. Alternatively, Sarkar et al. (1991) proposed

$$F(M_t) = M_t^2 \quad \text{and} \quad \xi^* = 1. \tag{8.121}$$

Wilcox (1992) discussed another form of $F(M_t)$ for both compressible mixing layers and boundary layers as

$$F(M_t) = (M_t - M_{t_o})^2 \mathcal{H}(M_t - M_{t_o}) \quad \text{and} \quad \xi^* = 2, \tag{8.122}$$

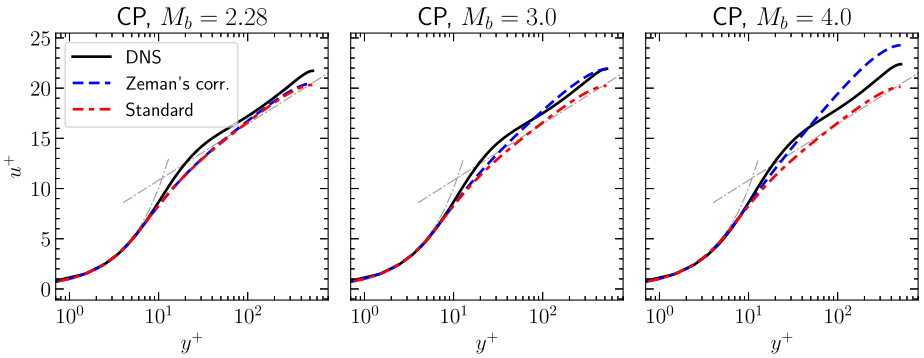

FIGURE 8.11 Mean-velocity profile computed using Menter's SST model with and without Zeman's dilatation–dissipation correction.

where M_{t_o} was set equal to 0.25.

For $k-\varepsilon$ models, in order to implement these corrections, only the dissipation term in k equation needs to be modified. However, for $k-\omega$ models, one also needs to modify the ω equation. Wilcox (1992) argued that the transport equation for ω should be considered as an equation for specific solenoidal-dissipation rate, namely, $\omega = \varepsilon_{M,s}/(\beta^* k)$. Consequently, they proposed to incorporate the dilatation–dissipation corrections by changing the model functions β^* in the destruction of TKE, and β in the destruction of ω to

$$\beta_c^* = \beta^* \left[1 + \xi^* F\left(M_t\right)\right], \quad \beta_c = \beta - \beta^* \xi^* F\left(M_t\right), \tag{8.123}$$

where the subscript 'c' indicates the correction to account for compressibility, whereas the constants without subscripts correspond to the standard values of the incompressible model, i.e., $\beta^* = 0.09$ and $\beta = 0.075$.

Wilcox (2006) applied the Wilcox dilatation–dissipation model for boundary layers and observed that the model increases the error in skin friction predictions as compared to an uncorrected model. On the other hand, Rumsey (2010) observed the Zeman's correction for boundary layers improves the accuracy, particularly for cold wall boundary layers. However, they suspected the improvement in the accuracy to be due to wrong reasons since the model does not capture the right physics.

Here, we test the dilatation–dissipation model of Zeman using a $k-\omega$ SST model (Menter, 1994) for the four constant-property compressible cases just discussed. Fig. 8.11 shows the mean-velocity profiles with and without Zeman's corrections. The correction is almost ineffective for the Mach 2.28 case. It improves the result for the Mach 3 case, however, for the Mach 4 case, the correction is too aggressive leading to a much higher velocity as compared to the DNS results. The main takeaway from this is that the correction tends to shift the log-law in the correct direction. This is because high-speed effects tend to reduce the eddy viscosity at a particular wall-normal location (due to an outward shift; see Fig. 8.9), and thus, increasing the dissipation, reduces turbulent kinetic energy, thus achieving the desired reduction in eddy viscosity.

8.5.3.2 Pressure dilatation

Sarkar (1992) modeled the pressure dilatation using the production and dissipation of turbulent kinetic energy as

$$\Pi_d = \alpha_2 P_k M_t + \alpha_3 \bar{\rho} \varepsilon_{M,s} M_t^2, \tag{8.124}$$

with P_k the turbulence production, $\alpha_2 = 0.15$ and $\alpha_3 = 0.2$. Zeman (1993) deduced a model specifically for boundary layers, in terms of the mean density gradient, as

$$\Pi_d = f(M_t) \left(\frac{d\bar{\rho}}{dy} \right)^2 \frac{k}{\varepsilon_{M,s}} \frac{\bar{a}^2}{\bar{\rho}} \widetilde{v''v''}, \tag{8.125}$$

where $\bar{a}$ is the local speed of sound and $f(M_t)$ is defined as[1]

$$f(M_t) = 0.02 \left(1 - \exp\left(-M_t^2 / 0.2 \right) \right). \tag{8.126}$$

This model requires the wall-normal Reynolds stress and is thus unsuitable for two-equation models. Some other models for Π_d have been proposed, for instance, by Ristorcelli (1997), however, there is no widely accepted form (Wilcox, 2006).

Huang et al. (1994) tested Sarkar's model for boundary layers and found that the log-law slope is overpredicted (lower effective von Kármán constant). On the other hand, Zeman (1993) tested their pressure–dilatation correction in a k-ε model for boundary layers and found an improvement of the results. However, the same model would be ineffective for the constant-property cases considered here due to the mean density being approximately constant ($d\bar{\rho}/dy \approx 0$).

While the dilatation–dissipation and pressure–dilatation models improve the results in some cases, their models fail to capture the right physics. This motivates the need to propose intrinsic compressibility corrections based on physical arguments.

8.5.3.3 Corrections based on damping functions

Inspired from the damping-function corrections for mixing-length models, Hasan et al. (2025b) proposed to modify the eddy viscosity of other two-equation turbulence models by multiplying the standard eddy-viscosity formulation with an appropriate damping function. They first rewrote the modified JK model as

$$\mu_t = \bar{\rho} u_\tau^* \kappa y D^2(y^*, M_\tau) = \bar{\rho} u_\tau^* \kappa y D^2(y^*, 0) \underbrace{\frac{D^2(y^*, M_\tau)}{D^2(y^*, 0)}}_{D^{ic}}, \tag{8.127}$$

where $\bar{\rho} u_\tau^* \kappa y D^2(y^*, 0)$ signifies a variable-property-corrected eddy-viscosity model and D^{ic} signifies the change in damping due to intrinsic compressibility effects. In order to account for intrinsic compressibility effects in two-equation models, a damping function analogous

[1] Note that $f(M_t)$ is wrongly stated in Zeman (1993) as pointed out by Huang et al. (1995).

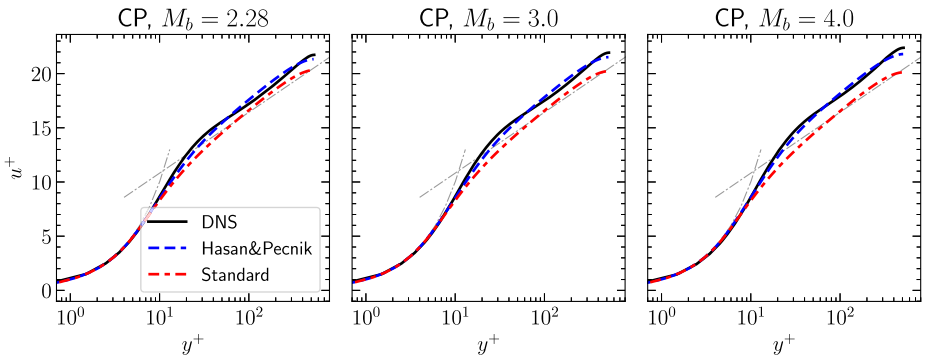

FIGURE 8.12 Mean-velocity profile computed using Menter's SST model with and without the damping-function correction of Hasan et al. (2025b).

to D^{ic} is required. Hasan et al. (2025b) proposed a damping function correction for the k-ω model as

$$\mu_t = \frac{\bar{\rho}k}{\omega} \underbrace{\frac{D^2(R_t, M_t)}{D^2(R_t, 0)}}_{(D^{ic})_{k\omega}}, \tag{8.128}$$

with

$$D(R_t, M_t) = 1 - \exp\left(\frac{-R_t}{K + f(M_t)}\right), \tag{8.129}$$

where M_t is the turbulence Mach number and $R_t = \bar{\rho}k/(\bar{\mu}\omega)$ is the turbulence Reynolds number, $K = 3.5$, and $f(M_t) = 0.39M_t^{0.77}$.

Fig. 8.12 shows the results with the k-ω SST model with and without the damping-function correction, for the four CP cases. Clearly, the results improve when the damping function in Eq. (8.128) is used.

The improvement in the results is not limited to the constant-property cases. The results also improve for a wide range of conventional turbulent boundary layers, as shown in Hasan et al. (2025b) (refer to the Jupyter-Notebook (Hasan and Pecnik, 2024) to replicate their results). This makes the damping function corrections to be a promising approach of accounting intrinsic compressibility effects in two-equation turbulence models.

8.6 Energy equation

The results presented in Sects. 8.4.4 and 8.4.5 were obtained using the mean density and viscosity profiles from the DNS. However, for practical applications, it is crucial to estimate these thermo-physical properties by solving the energy equation.

An alternative approach for high-speed flows is the use of well-established temperature–velocity relationships (Van Driest, 1951; Walz, 1969; Duan et al., 2011; Zhang et al., 2014).

These algebraic equations estimate the mean temperature based on the mean velocity, thereby enabling the estimation of mean properties. While these equations are highly accurate for canonical flat-plate boundary layers, they rely on boundary-layer-edge quantities, making them less suitable for applications, where only the inner layer is being solved (e.g., wall-modeled large eddy simulations) or for non-canonical cases (e.g., flows in complex geometries). For more details on these relationships, the reader is referred to Chap. 7.

In this chapter, we will focus on the modeling of the total energy equation (8.42). Revisiting Eq. (8.42), two key points are noted. First, the turbulent Prandtl number Pr_t is yet to be defined. Pr_t for high-speed flows involving ideal gases is often assumed to be constant throughout the domain, typically with a value of 0.9 (Wilcox, 2006). However, this assumption has recently been challenged by Griffin et al. (2023); Chen et al. (2024), especially in the context of cooled-wall boundary layers.

Second, the modeling of the molecular and turbulent diffusion of TKE needs to be updated based on the variable-property corrections discussed in Sect. 8.4.5. Particularly, the wall-normal (y) component of term (3) in Eq. (8.42) should be replaced with

$$\frac{1}{\bar{\mu}}\frac{d}{d(y\sqrt{\bar{\rho}}/\bar{\mu})}\left[\left(\mu+\frac{\mu_t}{\sigma_k}\right)\frac{1}{\bar{\mu}}\frac{d(\bar{\rho}k)}{d(y\sqrt{\bar{\rho}}/\bar{\mu})}\right]$$

in the inner layer, and with

$$\frac{1}{\sqrt{\bar{\rho}}}\frac{d}{dy}\left[\left(\bar{\mu}+\frac{\mu_t}{\sigma_k}\right)\frac{1}{\sqrt{\bar{\rho}}}\frac{d(\bar{\rho}k)}{dy}\right]$$

in the outer layer. Note that, in some studies, the TKE diffusion term is assumed to be negligible (Larsson et al., 2016; Bose and Park, 2018; Huang et al., 2023). By neglecting this term in the inner layer, it follows that the production of TKE is equal to its dissipation, which is a valid assumption in the log-layer, but not in the viscous sub- and the buffer-layer, where the production and dissipation terms are balanced with the total diffusion of turbulent kinetic energy.

To further clarify these issues, Hasan et al. (2025b) performed two tests: one related to the accurate modeling of Pr_t and the other related to the importance of including the TKE diffusion term in the energy equation. For the first test, they observed that the results with $Pr_t = 0.9$ and that with Pr_t taken from the DNS are almost identical, thereby concluding that $Pr_t = 0.9$ is a reasonable approximation for ideal-gas flows. In the second test, they found that including the TKE diffusion term estimated from the employed turbulence model ($k-\omega$ SST) was ineffective, as this model estimates zero diffusion values near the wall—whereas in reality, these values are non-zero. By incorporating a wall-dissipation component proposed by Rahman et al. (2012), which ensures non-zero dissipation (and hence non-zero diffusion) values at the wall, they achieved substantial improvement in the results, especially for cooled-wall boundary layers.

8.7 Concluding remarks

In conclusion, we have examined two key mechanisms in high-speed wall-bounded flows: variable-property effects due to heat transfer, which alter thermophysical properties such as density and viscosity, and intrinsic compressibility, which causes density variations in response to pressure fluctuations. It is essential that compressibility corrections in turbulence models capture both these mechanisms accurately. By distinguishing between variable-property effects and intrinsic compressibility, we can study them independently, allowing for the development of model corrections that reflect these underlying physics.

For variable-property effects, the most effective approach is to adjust turbulence models for mean property variations, ensuring consistency with the semi-local scaling framework. We discussed how this framework can guide the development of corrections for algebraic turbulence models and models based on transport equations. With these corrections, turbulence models are able to predict accurate velocity profiles for low Mach as well as for high Mach-number channel flows showcased in this chapter.

Regarding the direct effects of intrinsic compressibility in the turbulent kinetic energy (TKE) equation, mechanisms such as dilatation–dissipation and pressure-dilatation can be considered negligible, especially where the friction Mach numbers are below 0.2. Conversely, the indirect effects of intrinsic compressibility on turbulence quantities, such as turbulent shear stress, can be accounted for by empirically modifying the damping function. Future research should focus on how these variable property and intrinsic compressibility corrections perform in more general flow problems, including those involving shock waves, flow separation, and complex geometries.

References

Baldwin, Barrett, Lomax, Harvard, 1978. Thin-layer approximation and algebraic model for separated turbulent flows. In: 16th Aerospace Sciences Meeting, p. 257.

Blaisdell, G.A., Mansour, N.N., Reynolds, W.C., 1993. Compressibility effects on the growth and structure of homogeneous turbulent shear flow. Journal of Fluid Mechanics 256, 443–485.

Bose, Sanjeeb T., Park, George Ilhwan, 2018. Wall-modeled large-eddy simulation for complex turbulent flows. Annual Review of Fluid Mechanics 50, 535–561.

Bradshaw, Peter, 1977. Compressible turbulent shear layers. Annual Review of Fluid Mechanics 9 (1), 33–52.

Bradshaw, Peter, Huang, George P., 1995. The law of the wall in turbulent flow. Proceedings of the Royal Society of London. Series A, Mathematical and Physical Sciences 451 (1941), 165–188.

Bradshaw, Peter, Perot, J. Blair, 1993. A note on turbulent energy dissipation in the viscous wall region. Physics of Fluids. A, Fluid Dynamics 5 (12), 3305–3306.

Cabot, W., 1995. Large-eddy simulations with wall models. In: Center for Turbulence Research Annual Research Briefs: 1995.

Candler, Graham V., 2019. Rate effects in hypersonic flows. Annual Review of Fluid Mechanics 51 (1), 379–402. https://doi.org/10.1146/annurev-fluid-010518-040258.

Catris, Stéphane, Aupoix, Bertrand, 2000. Density corrections for turbulence models. Aerospace Science and Technology 4 (1), 1–11.

Chen, Xianliang, Gan, Jianping, Fu, Lin, 2024. An improved Baldwin–Lomax algebraic wall model for high-speed canonical turbulent boundary layers using established scalings. Journal of Fluid Mechanics 987, A7.

Chien, Kuei-Yuan, 1982. Predictions of channel and boundary-layer flows with a low-Reynolds-number turbulence model. AIAA Journal 20 (1), 33–38.

Coleman, Gary N., Kim, John, Moser, R.D., 1995. A numerical study of turbulent supersonic isothermal-wall channel flow. Journal of Fluid Mechanics 305, 159–183.
Duan, L., Beekman, I., Martin, M.P., 2010. Direct numerical simulation of hypersonic turbulent boundary layers. Part 2. Effect of wall temperature. Journal of Fluid Mechanics 655, 419–445.
Duan, L., Beekman, I., Martin, M.P., 2011. Direct numerical simulation of hypersonic turbulent boundary layers. Part 3. Effect of Mach number. Journal of Fluid Mechanics 672, 245–267.
Durbin, Paul A., 1995. Separated flow computations with the k-epsilon-v-squared model. AIAA Journal 33 (4), 659–664.
Favre, A., 1969. Statistical equations of turbulent gases. In: Problems of Hydrodynamics and Continuum Mechanics, pp. 231–266.
Foysi, H., Sarkar, S., Friedrich, R., 2004. Compressibility effects and turbulence scalings in supersonic channel flow. Journal of Fluid Mechanics 509, 207–216.
Friedrich, R., 1999. Modelling of turbulence in compressible flows. In: Hanifi, A., Alfredsson, P.H., Johansson, A.V., Henningson, D.S. (Eds.), Transition, Turbulence and Combustion Modelling: Lecture Notes from the 2nd ER-COFTAC Summerschool. Stockholm, 10–16 June, 1998. Springer Netherlands, Dordrecht. ISBN 978-94-011-4515-2, pp. 243–348.
Gatski, Thomas B., Bonnet, Jean-Paul, 2013. Compressibility, Turbulence and High Speed Flow. Academic Press.
Griffin, Kevin P., Fu, Lin, Moin, Parviz, 2023. Near-wall model for compressible turbulent boundary layers based on an inverse velocity transformation. Journal of Fluid Mechanics 970, A36.
Griffin, Kevin Patrick, Fu, Lin, Moin, Parviz, 2021. Velocity transformation for compressible wall-bounded turbulent flows with and without heat transfer. Proceedings of the National Academy of Sciences 118 (34), e2111144118.
Hasan, Asif Manzoor, Pecnik, Rene, 2024. Variable-property and intrinsic compressibility corrections for turbulence models using near-wall scaling theories. https://github.com/Fluid-Dynamics-Of-Energy-Systems-Team/RANS_Scaling2024.git.
Hasan, Asif Manzoor, Larsson, Johan, Pirozzoli, Sergio, Pecnik, Rene, 2023. Incorporating intrinsic compressibility effects in velocity transformations for wall-bounded turbulent flows. Physical Review Fluids 8, L112601.
Hasan, Asif Manzoor, Larsson, Johan, Pirozzoli, Sergio, Pecnik, Rene, 2024. Estimating mean profiles and fluxes in high-speed turbulent boundary layers using inner/outer-layer scalings. AIAA Journal 62 (2), 848–853.
Hasan, Asif Manzoor, Costa, Pedro, Larsson, Johan, Pirozzoli, Sergio, Pecnik, Rene, 2025a. Intrinsic compressibility effects in near-wall turbulence. Journal of Fluid Mechanics 1006, A14.
Hasan, Asif Manzoor, Elias, Alex Jose, Menter, Florian, Pecnik, Rene, 2025b. Variable-property and intrinsic compressibility corrections for turbulence models using near-wall scaling theories. Journal of Fluid Mechanics. In press.
Huang, P.G., Bradshaw, P., Coakley, T.J., 1994. Turbulence models for compressible boundary layers. AIAA Journal 32 (4), 735–740.
Huang, P.G., Coleman, G.N., Bradshaw, P., 1995. Compressible turbulent channel flows: DNS results and modelling. Journal of Fluid Mechanics 305, 185–218.
Huang, P.G., Coleman, G.N., Spalart, P.R., Yang, X.I.A., 2023. Velocity and temperature scalings leading to compressible laws of the wall. Journal of Fluid Mechanics 977, A49.
Iyer, Prahladh S., Malik, Mujeeb R., 2019. Analysis of the equilibrium wall model for high-speed turbulent flows. Physical Review Fluids 4 (7), 074604.
Johnson, Dennis A., King, L.S., 1985. A mathematically simple turbulence closure model for attached and separated turbulent boundary layers. AIAA Journal 23 (11), 1684–1692.
Kawai, Soshi, 2019. Heated transcritical and unheated non-transcritical turbulent boundary layers at supercritical pressures. Journal of Fluid Mechanics 865, 563–601.
Kovasznay, Leslie SG, 1953. Turbulence in supersonic flow. Journal of the Aeronautical Sciences 20 (10), 657–674.
Lagha, Maher, Kim, John, Eldredge, J.D., Zhong, Xiaolin, 2011. A numerical study of compressible turbulent boundary layers. Physics of Fluids 23 (1), 015106.
Larsson, Johan, Kawai, Soshi, Bodart, Julien, Bermejo-Moreno, Ivan, 2016. Large eddy simulation with modeled wall-stress: recent progress and future directions. Mechanical Engineering Reviews 3 (1), 15–00418.
Lechner, Richard, Sesterhenn, Joern, Friedrich, Rainer, 2001. Turbulent supersonic channel flow. Journal of Turbulence 2, 1–25.
Lele, Sanjiva K., 1994. Compressibility effects on turbulence. Annual Review of Fluid Mechanics 26 (1), 211–254.

Livescu, Daniel, 2020. Turbulence with large thermal and compositional density variations. Annual Review of Fluid Mechanics 52, 309–341.
Majda, Andfrew, Sethian, James, 1985. The derivation and numerical solution of the equations for zero Mach number combustion. Combustion Science and Technology 42 (3–4), 185–205.
Menter, Florian R., 1994. Two-equation eddy-viscosity turbulence models for engineering applications. AIAA Journal 32 (8), 1598–1605.
Modesti, Davide, Pirozzoli, Sergio, 2016. Reynolds and Mach number effects in compressible turbulent channel flow. International Journal of Heat and Fluid Flow 59, 33–49.
Morinishi, Y., Tamano, S., Nakabayashi, K., 2004. Direct numerical simulation of compressible turbulent channel flow between adiabatic and isothermal walls. Journal of Fluid Mechanics 502, 273–308.
Morkovin, M.V., 1962. Effects of compressibility on turbulent flows. In: Mecanique de la Turbulence, pp. 367–380.
Moser, Robert D., Kim, John, Mansour, Nagi N., 1999. Direct numerical simulation of turbulent channel flow up to $Re_\tau = 590$. Physics of Fluids 11 (4), 943–945.
Myong, H.K., Kasagi, N., 1990. A new approach to the improvement of k-e turbulence model for wall-bounded shear flows. JSME 33 (2).
Otero R., Gustavo J., Patel, Ashish, Diez S., Rafael, Pecnik, Rene, 2018. Turbulence modelling for flows with strong variations in thermo-physical properties. International Journal of Heat and Fluid Flow 73, 114–123.
Otero-Rodriguez, Gustavo, Smit, Stephan H.H.J., Pecnik, Rene, 2021. Three-dimensional unsteady stator-rotor interactions in high-expansion organic Rankine cycle turbines. Energy 217, 119339.
Pan, Shaowu, Johnsen, Eric, 2017. The role of bulk viscosity on the decay of compressible, homogeneous, isotropic turbulence. Journal of Fluid Mechanics 833, 717–744. https://doi.org/10.1017/jfm.2017.598.
Patel, A., Pecnik, R., Peeters, J.W.R., Hickel, S., Moghadam, M.E., 2016a. Turbulence modulation by variable density and viscosity. In: Proceedings of the Summer Program, p. 213.
Patel, Ashish, Peeters, Jurriaan W.R., Boersma, Bendiks J., Pecnik, Rene, 2015. Semi-local scaling and turbulence modulation in variable property turbulent channel flows. Physics of Fluids 27 (9), 095101.
Patel, Ashish, Boersma, Bendiks J., Pecnik, Rene, 2016b. The influence of near-wall density and viscosity gradients on turbulence in channel flows. Journal of Fluid Mechanics 809, 793–820.
Pecnik, R., Hasan, Asif M., 2023. Drag and heat transfer estimation. https://github.com/Fluid-Dynamics-Of-Energy-Systems-Team/DragandHeatTransferEstimation.git.
Pecnik, R., Hasan, A.M., Otero Rodriguez, G.J., 2023. Jupyter-notebook: RANS-models for compressible fully developed turbulent channel flows. https://github.com/Fluid-Dynamics-Of-Energy-Systems-Team/RANS_Channel.
Pecnik, Rene, Patel, Ashish, 2017. Scaling and modelling of turbulence in variable property channel flows. Journal of Fluid Mechanics 823, R1.
Piomelli, Ugo, Balaras, Elias, 2002. Wall-layer models for large-eddy simulations. Annual Review of Fluid Mechanics (ISSN 1545-4479) 34, 349–374.
Pope, Stephen B., 2000. Turbulent Flows. Cambridge University Press.
Pettersson Reif, B.A., Durbin, P.A., 2011. Statistical Theory and Modeling for Turbulent Flows. John Wiley & Sons.
Rahman, Md Mizanur, Wallin, Stefan, Siikonen, Timo, 2012. Exploring k and ϵ with R–equation model using elliptic relaxation function. Flow, Turbulence and Combustion 89 (1), 121–148. Springer.
Ristorcelli, J.R., 1993. A representation for the turbulent mass flux contribution to Reynolds-stress and two-equation closures for compressible turbulence. Technical report. Institute for Computer Applications in Science and Engineering Hampton Va.
Ristorcelli, J.R., 1997. A pseudo-sound constitutive relationship for the dilatational covariances in compressible turbulence. Journal of Fluid Mechanics 347, 37–70.
Rubesin, Morris W., 1990. Extra compressibility terms for favre-averaged two-equation models of inhomogeneous turbulent flows. Technical report, NASA CR-177556.
Rumsey, Christopher L., 2010. Compressibility considerations for kw turbulence models in hypersonic boundary-layer applications. Journal of Spacecraft and Rockets 47 (1), 11–20.
Sarkar, S., 1992. The pressure–dilatation correlation in compressible flows. Physics of Fluids. A, Fluid Dynamics 4 (12), 2674–2682.
Sarkar, Sutanu, Erlebacher, Gordon, Hussaini, M. Yousuff, Kreiss, Heinz Otto, 1991. The analysis and modelling of dilatational terms in compressible turbulence. Journal of Fluid Mechanics 227, 473–493.
Shadloo, M.S., Hadjadj, A., Hussain, Fazle, 2015. Statistical behavior of supersonic turbulent boundary layers with heat transfer at $M_\infty = 2$. International Journal of Heat and Fluid Flow 53, 113–134.

Shih, Tsan-Hsing, Lumley, John L., Janicka, J., 1987. Second-order modelling of a variable-density mixing layer. Journal of Fluid Mechanics 180, 93–116.
Smith, A.M.O., Cebeci, Tuncer, 1967. Numerical Solution of the Turbulent-Boundary-Layer Equations. Douglas Aircraft Company, Douglas Aircraft Division.
Smith, Brian, 1995. Prediction of hypersonic shock wave turbulent boundary layer interactions with the kl two equation turbulence model. In: 33rd Aerospace Sciences Meeting and Exhibit, p. 232.
Smits, Alexander J., Dussauge, Jean-Paul, 2006. Turbulent Shear Layers in Supersonic Flow. Springer Science & Business Media.
Spalart, Philippe, Allmaras, Steven, 1992. A one-equation turbulence model for aerodynamic flows. In: 30th Aerospace Sciences Meeting and Exhibit, p. 439.
Touber, Emile, 2019. Small-scale two-dimensional turbulence shaped by bulk viscosity. Journal of Fluid Mechanics 875, 974–1003. https://doi.org/10.1017/jfm.2019.531.
Trettel, Andrew, Larsson, Johan, 2016. Mean velocity scaling for compressible wall turbulence with heat transfer. Physics of Fluids 28 (2), 026102.
Van Driest, Edward R., 1951. Turbulent boundary layer in compressible fluids. Journal of the Aeronautical Sciences 18 (3), 145–160.
Van Driest, Edward R., 1956. On turbulent flow near a wall. Journal of the Aeronautical Sciences 23 (11), 1007–1011.
Viala, S., Aupoix, B., 1995. Compressible turbulent boundary layer modelling. In: The 2nd Joint ASME/JSME Fluids Engineering Conference and ASME/EALA 6th International Conference, ASME Fluids Engineering Division Summer Meeting. Hilton Head Island, S.C., August 13–18.
Vreman, Albertus Willem, Sandham, N.D., Luo, K.H., 1996. Compressible mixing layer growth rate and turbulence characteristics. Journal of Fluid Mechanics 320, 235–258.
Walz, Alfred, 1969. Boundary Layers of Flow and Temperature. MIT Press.
Wilcox, David C., 1992. Dilatation-dissipation corrections for advanced turbulence models. AIAA Journal 30 (11), 2639–2646.
Wilcox, D.C., 2006. Turbulence Modeling for CFD, 3rd edition. DCW Industries. ISBN 1928729088.
Yang, Xiang I.A., Lv, Yu, 2018. A semi-locally scaled eddy viscosity formulation for les wall models and flows at high speeds. Theoretical and Computational Fluid Dynamics 32 (5), 617–627.
Yu, Ming, Xu, Chun-Xiao, 2021. Compressibility effects on hypersonic turbulent channel flow with cold walls. Physics of Fluids 33 (7), 075106.
Yu, Ming, Xu, Chun-Xiao, Pirozzoli, Sergio, 2019. Genuine compressibility effects in wall-bounded turbulence. Physical Review Fluids 4 (12), 123402.
Yu, Ming, Liu, PengXin, Fu, YaLu, Tang, ZhiGong, Yuan, XianXu, 2022. Wall shear stress, pressure, and heat flux fluctuations in compressible wall-bounded turbulence, part I: one-point statistics. Physics of Fluids 34 (6), 065139.
Zeman, Otto, 1990. Dilatation dissipation: the concept and application in modeling compressible mixing layers. Physics of Fluids. A, Fluid Dynamics 2 (2), 178–188.
Zeman, Otto, 1993. A new model for super/hypersonic turbulent boundary layers. In: 31st Aerospace Sciences Meeting, p. 897.
Zhang, Chao, Duan, Lian, Choudhari, Meelan M., 2018. Direct numerical simulation database for supersonic and hypersonic turbulent boundary layers. AIAA Journal 56 (11), 4297–4311.
Zhang, You-Sheng, Bi, Wei-Tao, Hussain, Fazle, She, Zhen-Su, 2014. A generalized Reynolds analogy for compressible wall-bounded turbulent flows. Journal of Fluid Mechanics 739, 392–420.